iScience

CellPress
OPEN ACCESS

Article

# Hepatic *Huwe1* loss protects mice from non-alcoholic fatty liver disease through lipid metabolic rewiring

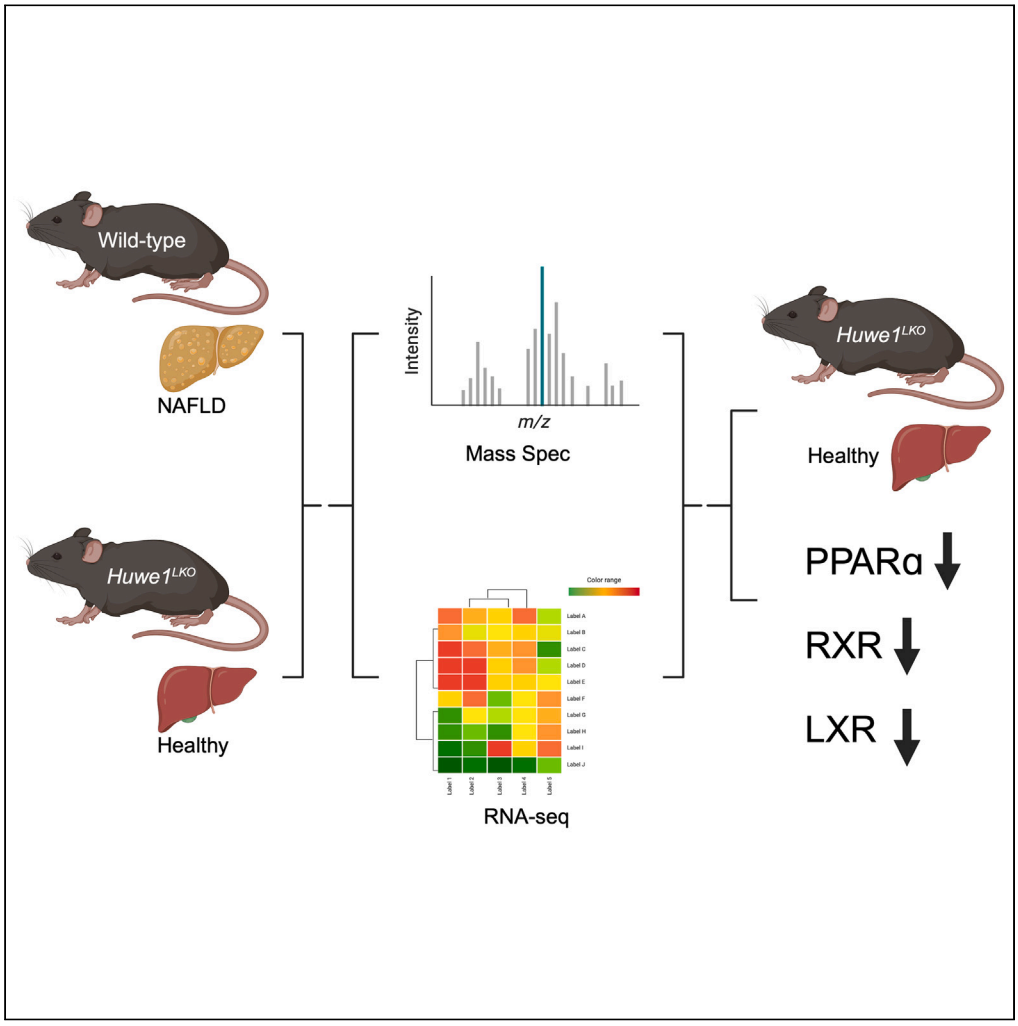


William W. Feng, Scott Bang, Eric M. Takacs, ..., Colleen M. Novak, Wei Gu, Manabu Kurokawa

mkurokaw@kent.edu

## Highlights

Liver-specific deletion of *Huwe1* prevents NAFLD induced by aging in mice

Liver-specific deletion of *Huwe1* also protects mice from diet-induced NAFLD

Mass spectrometry and RNA-seq analyses identified metabolic remodeling in *Huwe1* KO

ChEA analysis revealed downregulation of PPARα, LXR, and RXR activity in *Huwe1* KO

Feng et al., iScience *26*, 108405
December 15, 2023 
https://doi.org/10.1016/j.isci.2023.108405

iScience

CellPress
OPEN ACCESS

Article

# Hepatic *Huwe1* loss protects mice from non-alcoholic fatty liver disease through lipid metabolic rewiring

William W. Feng,[1,2,7,8] Scott Bang,[2,9] Eric M. Takacs,[2] Cora Day,[2] Katherine J. Crawford,[2,10] Ruba Al-Sheyab,[3] Dara B. Almufarrej,[3] Wendy Wells,[4] Serguei Ilchenko,[5] Takhar Kasumov,[5] Ning Kon,[6] Colleen M. Novak,[2,3] Wei Gu,[6] and Manabu Kurokawa[2,3,11,*]

## SUMMARY

**Non-alcoholic fatty liver disease (NAFLD) is the most pervasive liver pathology worldwide. Here, we demonstrate that the ubiquitin E3 ligase Huwe1 is vital in NAFLD pathogenesis. Using mass spectrometry and RNA sequencing, we reveal that liver-specific deletion of Huwe1 (*Huwe1*$^{LKO}$) in 1-year-old mice (approximately middle age in humans) elicits extensive lipid metabolic reprogramming that involves downregulation of *de novo* lipogenesis and fatty acid uptake, upregulation of fatty acid β-oxidation, and increased oxidative phosphorylation. ChEA transcription factor prediction analysis inferred these changes result from attenuated PPARα, LXR, and RXR activity in *Huwe1*$^{LKO}$ livers. Consequently, *Huwe1*$^{LKO}$ mice fed chow diet exhibited significantly reduced hepatic steatosis and superior glucose tolerance compared to wild-type mice. *Huwe1*$^{LKO}$ also conferred protection from high-fat diet-induced hepatic steatosis by 6-months of age, with increasingly robust differences observed as mice reached middle age. Together, we present evidence that Huwe1 plays a critical role in the development of age- and diet-induced NAFLD.**

## INTRODUCTION

Non-alcoholic fatty liver disease (NAFLD) is the most prevalent form of liver disease worldwide and is estimated to affect nearly a third of the population.[1] The hallmark characteristic of NAFLD is hepatic steatosis, or exacerbated lipid accumulation. Importantly, NAFLD is not a single disorder but rather encompasses a spectrum of liver diseases. NAFLD begins with the development of hepatic steatosis, but chronic inflammation mediates its progression into non-alcoholic steatohepatitis (NASH).[1,2] Subsequent liver damage, such as cirrhosis and fibrosis, then accrues over time and strongly predisposes individuals to hepatocellular carcinoma (HCC).[1–3] Several factors are known to contribute to the onset and progression of NAFLD-related disorders, including aging, obesity, hypertension, dyslipidemia, type 2 diabetes (T2DM), and metabolic syndrome.[1,3,4] Although hepatic steatosis seen in early NAFLD can be reversed with lifestyle interventions such as diet and exercise, liver damage brought on by cirrhosis and fibrosis is often regarded as irreversible. Because there are no Food and Drug Administration (FDA)-approved therapeutics for the treatment of NAFLD/NASH, there remains a critical need to identify strategies to prevent and reverse NAFLD-related pathologies.

Huwe1, also known as ARF-BP1, MULE, and HectH9, is a HECT (homology to E6-APC terminus)-domain E3 ubiquitin ligase originally identified as a binding partner of the tumor suppressor ARF (alternate reading frame; p14$^{ARF}$ in humans, p19$^{ARF}$ in mice), as well as a direct negative regulator of the tumor suppressor p53.[5] Overexpressed in a variety of cancer types, Huwe1 demonstrates an additional aspect of protumorigenicity by activating transcriptional activity of the proto-oncogene c-Myc via K-63 polyubiquitination.[6] Conversely, Huwe1 has also been shown to promote cancer cell apoptosis following DNA damage by facilitating the proteasomal degradation of MCL-1, an anti-apoptotic BCL-2 family member.[7] These seemingly contradictory observations illustrate that the role of Huwe1 *in vivo* is often complicated

[1]Department of Molecular and Systems Biology, Geisel School of Medicine at Dartmouth, Hanover, NH 03755, USA
[2]Department of Biological Sciences, Kent State University, Kent, OH 44242, USA
[3]School of Biomedical Sciences, Kent State University, Kent, OH 44240, USA
[4]Department of Pathology, Dartmouth-Hitchcock Medical Center, Lebanon, NH 03756, USA
[5]Department of Pharmaceutical Sciences, Northeast Ohio Medical University, Rootstown, OH 44272, USA
[6]Department of Pathology and Cell Biology, Columbia University, New York, NY 10032, USA
[7]Present address: Department of Medical Oncology, Dana-Farber Cancer Institute, Boston, MA 02215, USA
[8]Present address: Department of Medicine, Harvard Medical School, Boston, MA 02215, USA
[9]Present address: Department of Pharmacology, University of North Carolina, Chapel Hill, NC 27514, USA
[10]Present address: Department of Molecular and Cellular Biology, Roswell Park Comprehensive Cancer Center, Buffalo, NY 14263, USA
[11]Lead contact
*Correspondence: mkurokaw@kent.edu
https://doi.org/10.1016/j.isci.2023.108405

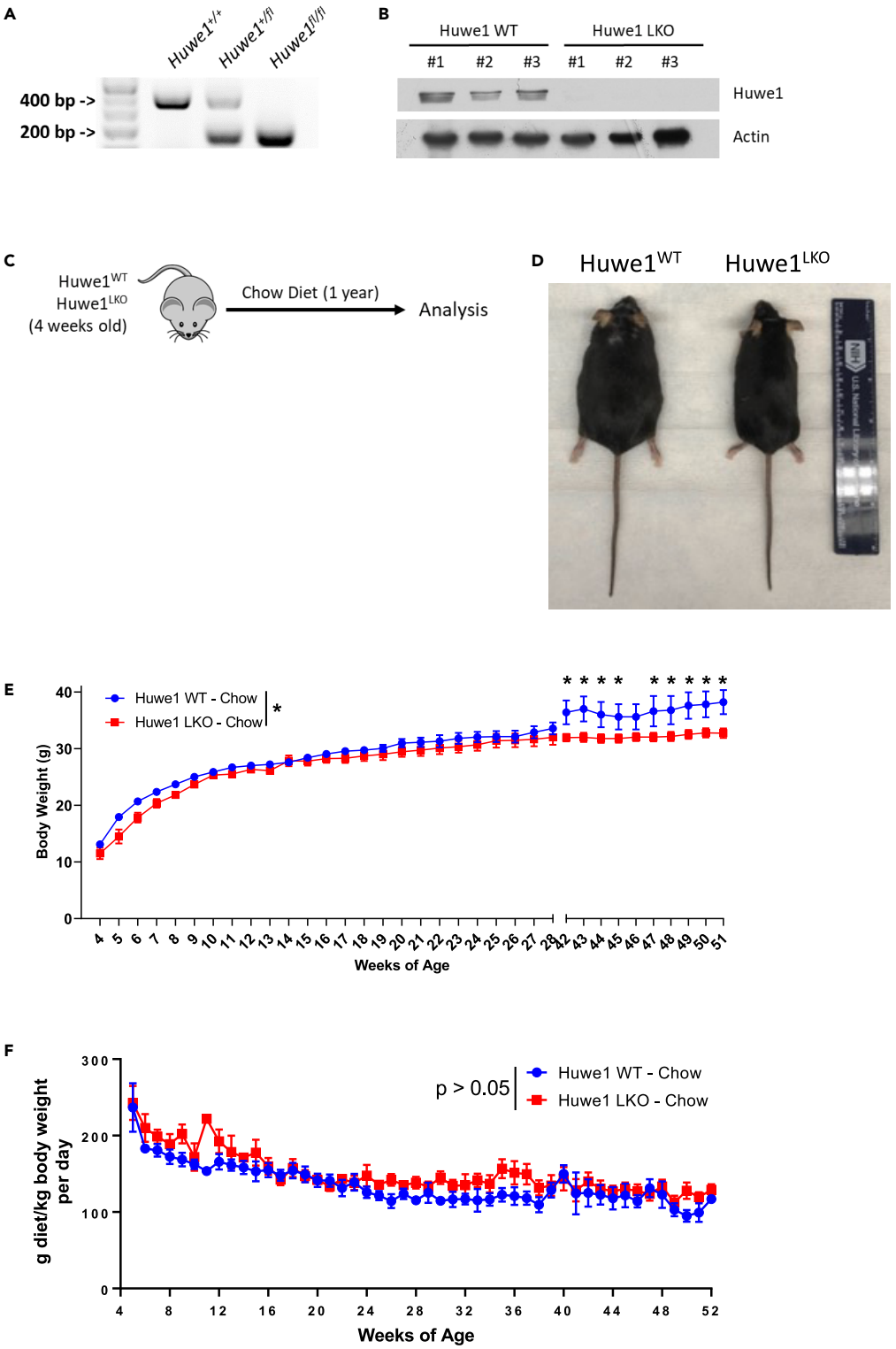


**Figure 1. Liver-specific deletion of *Huwe1* reduces body weight gain in 1-year-old mice**

(A) PCR genotyping results depicting the detection of wild-type and floxed *Huwe1* alleles in wild-type (*Huwe1*$^{+/+}$), heterozygous (*Huwe1*$^{+/fl}$), and homozygous floxed mice (*Huwe1*$^{fl/fl}$).

(B) Western blot confirming knockout efficiency in *Huwe1*$^{LKO}$ livers.

**Figure 1. *Continued***

(C) Schematic depicting the timeline of the diet study presented in D–F. *Huwe1*$^{WT}$ and *Huwe1*$^{LKO}$ body weight and food consumption were measured weekly starting at 4 weeks of age. This cohort of mice was evaluated over the span of 1 year. N = 15 mice per group.

(D) Representative photograph of 1-year-old *Huwe1*$^{WT}$ and *Huwe1*$^{LKO}$ mice.

(E and F) Body weight (E) and diet consumption (F) of *Huwe1*$^{WT}$ and *Huwe1*$^{LKO}$ mice maintained on chow diet for 1 year. Data are shown as mean ± SEM. See STAR Methods section for further detail of growth curve analysis.

due to the regulation of variable tissue-specific substrates with distinct context-dependent functions. For example, Huwe1 negatively regulates N-Myc in stem cells found in neural[8,9] and hematopoietic compartments[10] to inhibit proliferation, thereby maintaining stemness. In male germ cells, Huwe1 was found to play a critical role in spermatogenesis by ubiquitinating histones H1, H2A, H2B, H3, and H4 to regulate chromatin condensation.[11] Contrary to neural and hematopoietic stem cell populations, where inactivation of *Huwe1* promotes cellular proliferation and differentiation, *Huwe1* knockout in germ cells leads to a defect in spermatogenesis via hyperactivation of the DNA damage response pathway, and ultimately male infertility.[12,13] Moreover, we have previously demonstrated that oocyte-specific *Huwe1* knockout also renders female mice infertile, albeit via a p53-independent mechanism.[14] Therefore, the tissue-specific roles of Huwe1 remain heavily under investigation.

To characterize the *in vivo* role of Huwe1, we generated a liver-specific *Huwe1* (*Huwe1*$^{LKO}$) knockout mouse model. Surprisingly, liver-specific knockout of *Huwe1* protected mice from the development of age-induced hepatic steatosis. Mass spectrometry and RNA sequencing (RNA-seq) analyses of wild-type (*Huwe1*$^{WT}$) and *Huwe1*$^{LKO}$ mice revealed that *Huwe1*$^{LKO}$ resulted in marked downregulation of hepatic lipid metabolism genes and concomitant upregulation of genes related to mitochondrial fatty acid (FA) β-oxidation and oxidative phosphorylation. Accordingly, *Huwe1*$^{LKO}$ mice were also protected from high-fat diet (HFD)-induced development of hepatic steatosis and exhibited reduced accumulation of body fat percentage and body weight, in addition to lower incidence of HCC. *Huwe1*$^{LKO}$ mice also demonstrated resistance to developing glucose intolerance following prolonged HFD administration. Our results place Huwe1 as a novel regulator of age- and diet-induced NAFLD.

## RESULTS

### Liver-specific inactivation of Huwe1 attenuates the development of age-associated hepatic steatosis

We first generated a liver-specific *Huwe1* knockout mouse model by crossing previously established *Huwe1*$^{f/fl}$ mice[15] with mice expressing Cre recombinase under the control of the hepatocyte-specific albumin promoter (*Alb-cre*)[16] (Figure 1A). Although the global deletion of *Huwe1* is known to be embryonically lethal,[14,15] liver-specific inactivation allowed for the development of viable pups. Western blot of liver tissue lysates was performed to confirm knockout efficiency in *Huwe1*$^{LKO}$ mice (Figure 1B). To investigate the physiological role of hepatic Huwe1, we measured the body weights of *Huwe1*$^{WT}$ and *Huwe1*$^{LKO}$ mice maintained on a standard chow diet over the span of 1 year (Figure 1C). Although no differences in body weight were observed earlier in life, a statistically significant 15% reduction in body weight was observed in *Huwe1*$^{LKO}$ mice relative to *Huwe1*$^{WT}$ as they became 1 year old (approximately equivalent to middle age in humans[17] [Figures 1D and 1E]). Importantly, the modest reduction in body weight was not attributed to differences in diet consumption (Figure 1F).

Interestingly, 1-year-old *Huwe1*$^{LKO}$ mice presented significantly smaller livers as compared to their wild-type counterparts although no difference was observed at 24 weeks of age (Figures 2A and 2B). Because aging is a prominent risk factor for the development of hepatic steatosis, we next histologically evaluated the liver morphology of 1-year-old mice. Hematoxylin and eosin (H&E) staining revealed that livers from 1-year-old *Huwe1*$^{LKO}$ mice exhibited profoundly less macrovesicular steatosis as compared to *Huwe1*$^{WT}$ livers (Figure 2C). Moreover, Oil Red O (ORO) staining confirmed that *Huwe1*$^{LKO}$ livers from 1-year-old mice exhibited a marked reduction in lipid droplet accumulation (Figure 2D). In addition, hepatic triglyceride (Figure 2E) and cholesterol (Figure 2F) levels were significantly reduced in 1-year-old *Huwe1*$^{LKO}$ livers as compared to *Huwe1*$^{WT}$. Since NAFLD prevalence in humans also peaks in middle age (~30–50 years old),[18] the kinetics of hepatic steatosis onset in *Huwe1*$^{WT}$ mice recapitulates the temporal etiology of the human disease. Interestingly, the protein expression levels of both FA synthase (FASN) and the FA transporter CD36 were markedly downregulated in 1-year-old *Huwe1*$^{LKO}$ livers, although the level of carnitine palmitoyl transferase I (CPT1), the rate-limiting enzyme of FA oxidation, appeared to be unaffected by *Huwe1*$^{LKO}$ (Figure 2G). These results suggest that Huwe1 plays a critical role in the development of age-associated NAFLD in part through diminished *de novo* lipogenesis and FA uptake.

### Huwe1$^{LKO}$ results in downregulation of *de novo* lipogenesis and upregulation of mitochondrial β-oxidation

Huwe1 is an E3 ubiquitin ligase with a wide range of substrates which often varies based on the context, such as tissue type. To elucidate the mechanism underlying the healthy liver phenotype observed in *Huwe1*$^{LKO}$ mice, we next performed mass spectrometry analysis on livers harvested from 1-year-old mice. A total of 710 proteins were detected in both *Huwe1*$^{WT}$ and *Huwe1*$^{LKO}$ livers (Figure 3A). Additionally, 190 proteins were measurable only in *Huwe1*$^{WT}$ livers and 341 proteins were found solely in *Huwe1*$^{LKO}$ livers. However, many of these proteins were detected with low abundance or inconsistently across replicates. We then sought to identify differentially expressed proteins between *Huwe1*$^{WT}$ and *Huwe1*$^{LKO}$ livers with a log2 fold change (log2FC) of $|\log2FC| > 0.5$ and a p value of $p < 0.05$ (Figure 3B). Using these parameters, we identified 82 proteins to be significantly enriched in *Huwe1*$^{LKO}$ livers (including 4 *Huwe1*$^{LKO}$-specific proteins) and 45 proteins to be significantly depleted in *Huwe1*$^{LKO}$ livers (including 8 *Huwe1*$^{WT}$-specific proteins). Gene set enrichment analysis revealed that "Hallmark_Fatty_Acid_Metabolism" was the most significantly upregulated (Figure S1A [*Huwe1*$^{LKO}$ livers from 1-year-old mice exhibit enrichment of metabolic

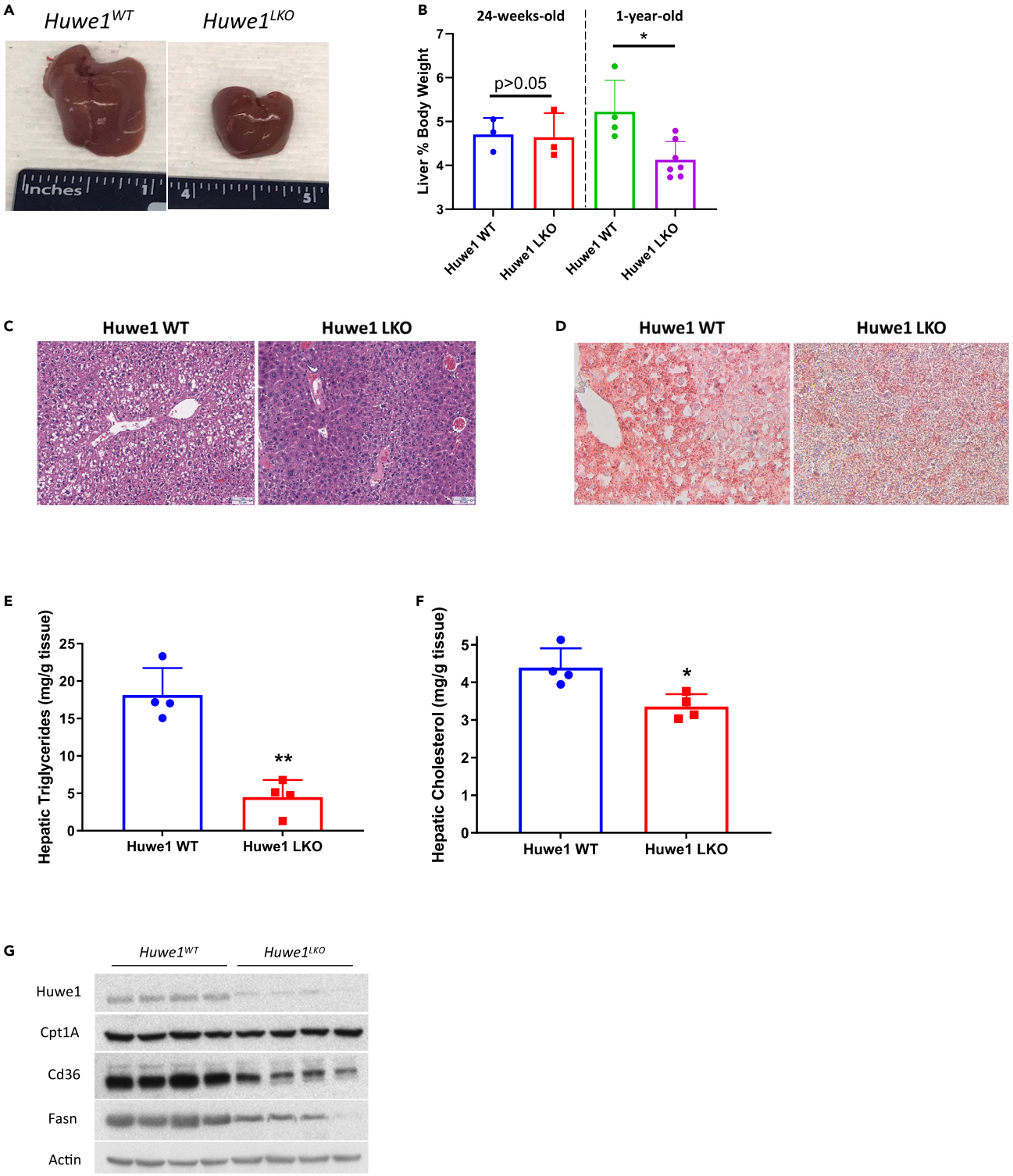


**Figure 2. Liver-specific deletion of *Huwe1* reduces liver size and lipid accumulation in 1-year-old mice**

(A) Representative photographs of livers from 1-year-old *Huwe1*$^{WT}$ and *Huwe1*$^{LKO}$ mice.

(B) *Huwe1*$^{LKO}$ mice exhibit no change in liver size relative to *Huwe1*$^{WT}$ at 24 weeks of age but a significant reduction at 1 year of age. Liver weights were normalized to body weight at each time point.

**Figure 2. *Continued***

(C and D) H&E (C) and ORO (D) staining of liver sections from middle-aged mice.

(E and F) Biochemical analysis measuring triglyceride (E) and cholesterol (F) in livers from 1-year-old mice. Data shown as mean +SD. Significance assessed by two-sided Student's *t* test with significance set at * <0.05, ** <0.005.

(G) Western blot was performed for the indicated proteins in livers isolated from 1-year-old *Huwe1*$^{WT}$ and *Huwe1*$^{LKO}$ mice.

proteins and pathways]) and downregulated pathway (Figure 3C) in *Huwe1*$^{LKO}$ livers. Indeed, we observed that several differentially expressed proteins in *Huwe1*$^{LKO}$ livers had roles in various aspects of lipid metabolism, including FA synthesis (AACS, ACACA/ACC1, ACACB/ACC2, ACLY, ACSA/ACSS2, FASN, MAOX/ME1), FA β-oxidation (ACADL, ACADV/ACADVL, EXHB/HADHB, THIM/ACAA2), lipid transfer (FABPL/FABP1, STARD10), and bile acid synthesis (CP270/CYP2C70, CP240/CYP2C40) (Figure 3D; Figure S1B [*Huwe1*$^{LKO}$ livers from 1-year-old mice exhibit enrichment of metabolic proteins and pathways]; Table S1 [Significantly enriched proteins in *Huwe1*$^{LKO}$ livers]; Table S2. [Significantly depleted proteins in *Huwe1*$^{LKO}$ livers]).

Upon closer scrutiny, we observed downregulation of nearly the entire *de novo* lipogenic pathway in the *Huwe1*$^{LKO}$ livers (Figures 3D and 3E). Particularly, two of the most highly depleted proteins were ACACA and ACACB (Figures 3B and 3D). These proteins catalyze the same irreversible carboxylation of acetyl-coenzyme A (CoA) to malonyl-CoA but differ in their subcellular localizations and functional consequences of their activities (Figure 3E). Specifically, mitochondrial ACACB produces malonyl-CoA to serve as a potent allosteric inhibitor of CPT1, a process which acts as a molecular switch to favor FA synthesis over catabolism. ACACA is the cytosolic isoform which produces malonyl-CoA in the rate limiting step of *de novo* FA synthesis. FASN then catalyzes the synthesis of FAs from malonyl-CoA and acetyl-CoA through multiple cycles of elongation reactions (Figure 3E). Consistent with our earlier result (Figure 2G), FASN was also markedly depleted in *Huwe1*$^{LKO}$ livers (Figures 3B and 3D). Furthermore, we also observed decreased expression of ACLY and ACSS2 (Figures 3B and 3D), which catalyze the synthesis of the lipogenesis substrate acetyl-CoA from citrate and acetate, respectively (Figure 3E).

In addition to the robust downregulation of the lipogenesis pathway, *Huwe1*$^{LKO}$ livers showed concomitant increased abundance of proteins involved in FA β-oxidation (ACAA2, ACADL, ACADVL, HADHB), tricarboxylic acid (TCA) cycle (IDHP/IDH2 and ODO1/OGDH), and glutaminolysis (GLSL/GLS2 and DHE3/GLUD1) (Figure 3E; Figure S1B [*Huwe1*$^{LKO}$ livers from 1-year-old mice exhibit enrichment of metabolic proteins and pathways]; Table S1 [Significantly enriched proteins in *Huwe1*$^{LKO}$ livers]). We also found the electron transfer flavoprotein ETFB and ATP synthase subunit F1 alpha (ATP5F1A) to be upregulated in *Huwe1*$^{LKO}$ livers (Table S1 [Significantly enriched proteins in *Huwe1*$^{LKO}$ livers]). ETFB facilitates the transfer of electrons from multiple flavoprotein dehydrogenases involved in FA β-oxidation and delivers them to NADH:ubiquinone oxidoreductase (Complex I) of the electron transport chain (ETC),[19] while ATP synthase (Complex V) catalyzes the final step of the ETC to generate ATP (Figure 3E). Interestingly, in contrast to the upregulation of mitochondrial FA β-oxidation enzymes in *Huwe1*$^{LKO}$ livers, we observed concurrent downregulation of peroxisomal β-oxidation enzymes (ABCD3, ECHP/EHHADH, THIKB/ACAA1B) (Figures 3C and 3D; Table S2 [Significantly depleted proteins in *Huwe1*$^{LKO}$ livers]). Together, these findings demonstrate that liver-specific deletion of *Huwe1* results in profound lipid metabolic reprogramming that involves significant downregulation of *de novo* FA lipogenesis and peroxisomal FA metabolism, in addition to marked upregulation of mitochondrial FA β-oxidation and oxidative phosphorylation.

## Huwe1$^{LKO}$ leads to lipid metabolic reprogramming at a transcriptional level

Because the loss of *Huwe1* should result in stabilization of its substrates, we reasoned that this could not explain the drastic downregulation of the entire FA synthesis pathway in 1-year-old *Huwe1*$^{LKO}$ livers. We then asked whether the extensive metabolic rewiring observed by our mass spectrometry analysis on *Huwe1*$^{LKO}$ livers was the result of a deregulated transcription factor in the absence of Huwe1. To this end, we interrogated our list of 127 differentially expressed proteins identified by mass spectrometry analysis and performed chromatin immunoprecipitation (ChIP) enrichment analysis (ChEA) using Enrichr.[20] ChEA is a powerful technique which leverages previously published chromatin immunoprecipitation (ChIP sequencing, ChIP-ChIP, ChIP-PET; ChIP-paired-end-ditag) and DNA adenine methyltransferase identification (DamID)[21] genome-wide mapping studies to define associations between transcription factors and their target genes.[22] ChEA then uses these annotations to infer enrichment of transcription factor activity for a gene set curated by the user.[22] Strikingly, ChEA analysis revealed a strong enrichment of PPARα, RXR, and LXR as predicted upstream regulators of differentially regulated genes in *Huwe1*$^{LKO}$ livers (Figure 3F; Table S3 [ChEA enrichment analysis on differentially expressed proteins in *Huwe1*$^{LKO}$ livers]). These three transcription factors belong to a common family of ligand-activated nuclear receptors that collectively serve as master regulators of hepatic lipid homeostasis. Moreover, it is known that the PPARα and LXR receptors form obligate heterodimers with RXR receptors, highlighting their intertwining activities.[23,24]

We evaluated the regulatory network predicted by ChEA analysis and found 21 genes to be commonly regulated by LXR, RXR, and PPARα, 10 genes regulated by LXR and RXR, and 9 genes regulated by PPARα and RXR (Figure 3G). Many of the dysregulated lipid metabolism genes previously identified by our mass spectrometry analysis were recapitulated in these three gene lists and were commonly regulated by all 3 transcription factors (Figure 3G; Table S3 [ChEA enrichment analysis on differentially expressed proteins in *Huwe1*$^{LKO}$ livers]). Furthermore, many of these dysregulated lipid metabolism genes were specifically involved in FA synthesis and peroxisomal FA β-oxidation (Figure 3G; Table S3 [ChEA enrichment analysis on differentially expressed proteins in *Huwe1*$^{LKO}$ livers]). Although *Huwe1*$^{LKO}$ did not affect protein levels of PPARα and LXR, we observed a subtle decrease in RXRα expression in mice as young as 2-months-old (Figure 3H). RXRα expression remains modestly diminished in 1-year-old *Huwe1*$^{LKO}$ mouse livers (Figure 3H).

To get a better sense of the transcriptional landscape of 1-year-old *Huwe1*$^{LKO}$ livers, we next performed bulk RNA-seq on livers collected from 1-year-old mice. We identified 524 upregulated and 618 downregulated genes in *Huwe1*$^{LKO}$ livers with a |log2FC| > 0.5

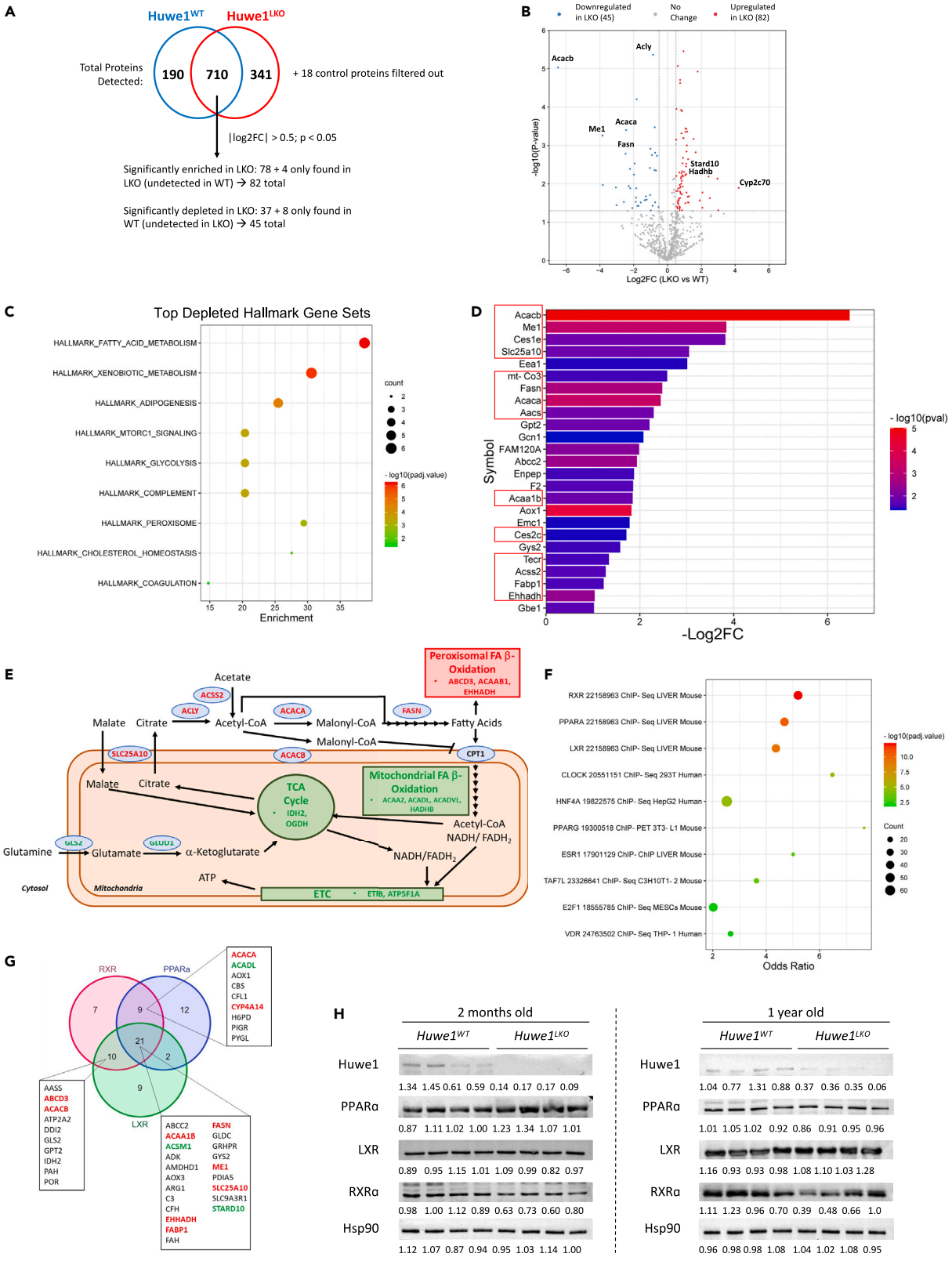
A
Huwe1WT
Huwe1LKO
Total Proteins Detected:
190
710
341
+ 18 control proteins filtered out
|log2FC| > 0.5; p < 0.05
Significantly enriched in LKO: 78 + 4 only found in LKO (undetected in WT) → 82 total
Significantly depleted in LKO: 37 + 8 only found in WT (undetected in LKO) → 45 total
B
Downregulated in LKO (45)
No Change
Upregulated in LKO (82)
Acacb
Acly
Me1
Acaca
Fasn
Stard10
Hadhb
Cyp2c70
-log10(P-value)
Log2FC (LKO vs WT)
C
Top Depleted Hallmark Gene Sets
HALLMARK_FATTY_ACID_METABOLISM
HALLMARK_XENOBIOTIC_METABOLISM
HALLMARK_ADIPOGENESIS
HALLMARK_MTORC1_SIGNALING
HALLMARK_GLYCOLYSIS
HALLMARK_COMPLEMENT
HALLMARK_PEROXISOME
HALLMARK_CHOLESTEROL_HOMEOSTASIS
HALLMARK_COAGULATION
count
- log10(padj.value)
Enrichment
D
Acacb
Me1
Ces1e
Slc25a10
Eea1
mt- Co3
Fasn
Acaca
Aacs
Gpt2
Gcn1
FAM120A
Abcc2
Enpep
F2
Acaa1b
Aox1
Emc1
Ces2c
Gys2
Tecr
Acss2
Fabp1
Ehhadh
Gbe1
Symbol
-Log2FC
- log10(pval)
E
Peroxisomal FA β-Oxidation
ABCD3, ACAAB1, EHHADH
Acetate
ACSS2
ACLY
Malate
Citrate
Acetyl-CoA
ACACA
Malonyl-CoA
FASN
Fatty Acids
SLC25A10
ACACB
CPT1
TCA Cycle
IDH2, OGDH
Mitochondrial FA β-Oxidation
ACAA2, ACADL, ACADVL, HADHB
Acetyl-CoA
NADH/ FADH2
Glutamine
GLS2
Glutamate
GLUD1
α-Ketoglutarate
ATP
ETC
ETFB, ATP5F1A
Cytosol
Mitochondria
F
RXR 22158963 ChIP- Seq LIVER Mouse
PPARA 22158963 ChIP- Seq LIVER Mouse
LXR 22158963 ChIP- Seq LIVER Mouse
CLOCK 20551151 ChIP- Seq 293T Human
HNF4A 19822575 ChIP- Seq HepG2 Human
PPARG 19300518 ChIP- PET 3T3- L1 Mouse
ESR1 17901129 ChIP- ChIP LIVER Mouse
TAF7L 23326641 ChIP- Seq C3H10T1- 2 Mouse
E2F1 18555785 ChIP- Seq MESCs Mouse
VDR 24763502 ChIP- Seq THP- 1 Human
- log10(padj.value)
Count
Odds Ratio
G
RXR
PPARa
LXR
7
9
12
21
10
2
9
ACACA
ACADL
AOX1
CBS
CFL1
CYP4A14
H6PD
PIGR
PYGL
AASS
ABCD3
ACACB
ATP2A2
DDI2
GLS2
GPT2
IDH2
PAH
POR
ABCC2
ACAA1B
ACSM1
ADK
AMDHD1
AOX3
ARG1
C3
CFH
EHHADH
FABP1
FAH
FASN
GLDC
GRHPR
GYS2
ME1
PDIA5
SLC25A10
SLC9A3R1
STARD10
H
2 months old
1 year old
Huwe1WT
Huwe1LKO
Huwe1
PPARα
LXR
RXRα
Hsp90
1.34 1.45 0.61 0.59 0.14 0.17 0.17 0.09
0.87 1.11 1.02 1.00 1.23 1.34 1.07 1.01
0.89 0.95 1.15 1.01 1.09 0.99 0.82 0.97
0.98 1.00 1.12 0.89 0.63 0.73 0.60 0.80
1.12 1.07 0.87 0.94 0.95 1.03 1.14 1.00
1.04 0.77 1.31 0.88 0.37 0.36 0.35 0.06
1.01 1.05 1.02 0.92 0.86 0.91 0.95 0.96
1.16 0.93 0.93 0.98 1.08 1.10 1.03 1.28
1.11 1.23 0.96 0.70 0.39 0.48 0.66 1.0
0.96 0.98 0.98 1.08 1.04 1.02 1.08 0.95

**Figure 3. Mass spectrometry analysis reveals drastic metabolic remodeling in *Huwe1*$^{LKO}$ livers from 1-year-old mice**

(A) Venn diagram listing total number of proteins detected in *Huwe1*$^{WT}$ and *Huwe1*$^{LKO}$ livers by mass spectrometry. |log2FC| > 0.5 and p < 0.05 thresholds were set for filtering of significant differentially expressed proteins.

(B) Volcano plot depicting differentially expressed proteins in *Huwe1*$^{WT}$ and *Huwe1*$^{LKO}$ livers.

(C) Hallmark gene set enrichment analysis was performed on the 45 significantly depleted proteins from *Huwe1*$^{LKO}$ livers using MSigDB.

(D) Bar graph showing the top 25 depleted proteins from *Huwe1*$^{LKO}$ livers sorted by -log2FC. Notably, many of these proteins were related to lipid metabolism or associated pathways (highlighted in red boxes).

(E) Signaling diagram depicting upregulated (green) and downregulated (red) proteins and metabolic processes in *Huwe1*$^{LKO}$ livers.

(F and G) ChEA analysis on all 127 differentially expressed proteins in *Huwe1*$^{LKO}$ livers revealed strong enrichment of RXR, PPARα, and LXR activity (F). Many of the differentially expressed proteins in *Huwe1*$^{LKO}$ livers are predicted to be regulated by RXR, PPARα, and/or LXR (G). Upregulated (Green) and downregulated (Red) proteins related to fatty acid metabolism are highlighted.

(H) Western blot was performed for the indicated proteins in livers isolated from 2-month-old and 1-year-old *Huwe1*$^{WT}$ and *Huwe1*$^{LKO}$ mice. Band densitometric values shown indicate Hsp90-normalized expression values relative to average expression of *Huwe1*$^{WT}$ samples.

and a Benjamini-Hochberg corrected p value (p.adj) of q < 0.05 (Figures 4A and 4B; Table S4 [Significantly enriched mRNA transcripts in *Huwe1*$^{LKO}$ livers]; Table S5 [Significantly depleted mRNA transcripts in *Huwe1*$^{LKO}$ livers]). As with our proteomics analysis, we observed several of the top downregulated pathways in *Huwe1*$^{LKO}$ livers were again related to lipid metabolism (Figure 4C). Specifically, we observed several of the lipogenesis genes identified to be depleted in *Huwe1*$^{LKO}$ livers by mass spectrometry were also downregulated at the mRNA level (*Aacs*, *Acaca*, *Acacb*, *Acly*, *Acss2*, *Fasn*, *Me1*) (Figure 4D; Table S5 [Significantly depleted mRNA transcripts in *Huwe1*$^{LKO}$ livers]). Unlike what we saw with the mass spectrometry analysis of *Huwe1*$^{LKO}$ livers, we surprisingly observed no change in mRNA levels of FA β-oxidation genes, lipid transfer genes, or bile synthesis genes (Figures S2A and S2B [*Huwe1*$^{LKO}$ livers from 1-year-old mice do not exhibit enrichment of lipid metabolic genes and pathways] and Table S4 [Significantly enriched mRNA transcripts in *Huwe1*$^{LKO}$ livers]). Notably, although Huwe1 is an E3 ligase for p53, hepatic depletion of *Huwe1* did not result in a significant induction of p53 target genes (Figure S2C [*Huwe1*$^{LKO}$ livers from 1-year-old mice do not exhibit enrichment of lipid metabolic genes and pathways]).

Consistent with our mass spectrometry results, our ChEA analysis on the 1,142 differentially expressed genes identified by RNA-seq showed significant enrichment for LXR, RXR, and PPARα activity in *Huwe1*$^{LKO}$ livers (Figures 4E and 4F; Table S6 [ChEA enrichment analysis on differentially expressed mRNA transcripts in *Huwe1*$^{LKO}$ livers]). We identified 76 genes to be commonly regulated by LXR, RXR, and PPARα, 60 genes regulated by LXR and RXR, and 67 genes regulated by PPARα-RXR (Figure 4F). In concordance with the ChEA analysis performed on the mass spectrometry samples, we detected a striking downregulation of lipid metabolism genes in these gene sets, again with the highest degree of enrichment seen in genes commonly regulated by LXR, RXR, and PPARα (Figure 4F; Table S6 [ChEA enrichment analysis on differentially expressed mRNA transcripts in *Huwe1*$^{LKO}$ livers]). These results suggest that metabolic reprogramming may occur in *Huwe1*$^{LKO}$ livers due to attenuated LXR/RXR/PPARα-dependent transcription, as well as LXR/RXR/PPARα-independent post-translational stabilization of Huwe1 substrates.

## Liver-specific Huwe1 knockout protects against diet-induced NAFLD but not obesity in 24-week-old mice

We next sought to determine whether the robust differential transcriptional and post-translational lipid metabolic gene signatures observed in *Huwe1*$^{LKO}$ livers could also confer protection from diet-induced hepatic steatosis. To this end, we challenged 4-week-old mice with HFD (45% kcal fat) or low-fat diet (LFD, 10% kcal fat) *ad libitum* for 20 weeks (Figure 5A). Although HFD significantly promoted increased weight gain in both genotypes as compared to respective mice on LFD, no differences in body weight were seen between genotypes within each diet group (Figure 5B). A 5% reduction in body weight was observed in *Huwe1*$^{LKO}$ mice on HFD relative to *Huwe1*$^{WT}$ mice on HFD at the end of the study. However, the differences did not reach statistical significance (p = 0.19; Figure 5B). As seen with the mice raised on chow diet (Figure 1F), LFD- and HFD-fed mice did not exhibit differences in diet consumption between genotypes in both diet groups (Figure 5C). Notably, while HFD induced an increase in the size of subcutaneous inguinal white adipose tissue (iWAT) in *Huwe1*$^{WT}$ mice, this diet effect was attenuated in *Huwe1*$^{LKO}$ mice (Figure 5D). However, no difference in visceral epididymal white adipose tissue (eWAT) was observed (Figure 5E). While HFD induced an increased mass of intrascapular brown adipose tissue (iBAT) in *Huwe1*$^{WT}$ mice, *Huwe1*$^{LKO}$ mice did not exhibit this effect (Figure 5F).

Although these 24-week-old *Huwe1*$^{LKO}$ mice were not protected from diet-induced obesity, liver-specific *Huwe1* deletion still conferred resistance against the development of diet-induced hepatic steatosis. HFD-fed *Huwe1*$^{LKO}$ livers were visually less mottled and lipid laden (Figure 5G). Indeed, *Huwe1*$^{LKO}$ mice were protected from HFD-induced increase in liver size, though no difference was observed in liver size between mice fed with LFD (Figure 5H). H&E and ORO stains confirmed less lipid accumulation in the livers of HFD-fed *Huwe1*$^{LKO}$ mice compared to those of HFD-fed *Huwe1*$^{WT}$ mice (Figure 5I). Moreover, this result corresponded with significantly reduced hepatic triglyceride content in HFD-fed *Huwe1*$^{LKO}$ mice compared to HFD-fed *Huwe1*$^{WT}$ mice (Figure 5J). These findings suggest that young *Huwe1*$^{LKO}$ mice are protected from diet-induced hepatic steatosis, but not from total weight gain.

## Liver-specific Huwe1 knockout protects against diet-induced NAFLD and diabetes in 1-year-old mice

It is well established that aging is a prominent contributing factor to the development of NAFLD and diet-induced hepatic steatosis.[4,25] Therefore, we sought to determine whether the protective phenotype observed in HFD-fed 24-week-old *Huwe1*$^{LKO}$ mice (Figure 5A) could be better recapitulated in 1-year-old mice, the setting where NAFLD prevalence peaks in humans.[18] To this end, we challenged 24-week-old mice

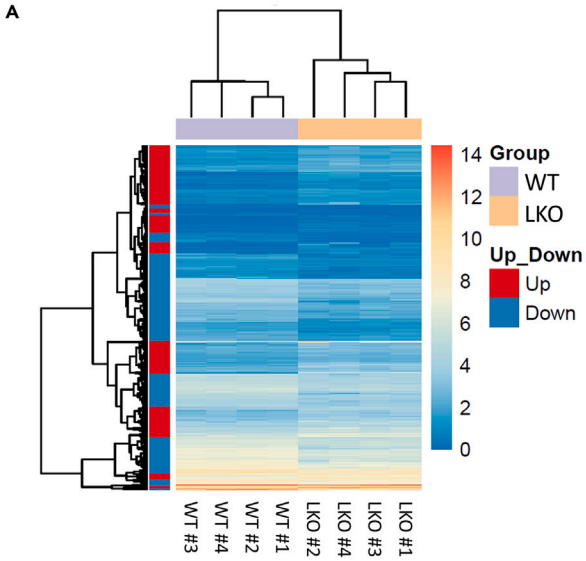
A
Group
WT
LKO
Up_Down
Up
Down
14
12
10
8
6
4
2
0
WT #3
WT #4
WT #2
WT #1
LKO #2
LKO #4
LKO #3
LKO #1

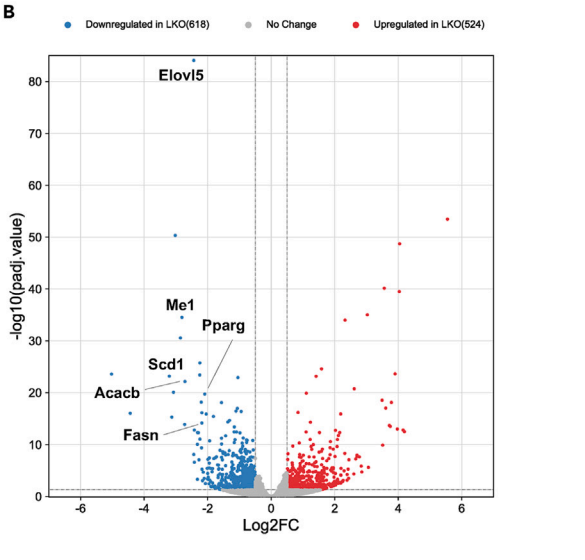
B
Downregulated in LKO(618)
No Change
Upregulated in LKO(524)
Elovl5
Me1
Pparg
Scd1
Acacb
Fasn
-log10(padj.value)
Log2FC

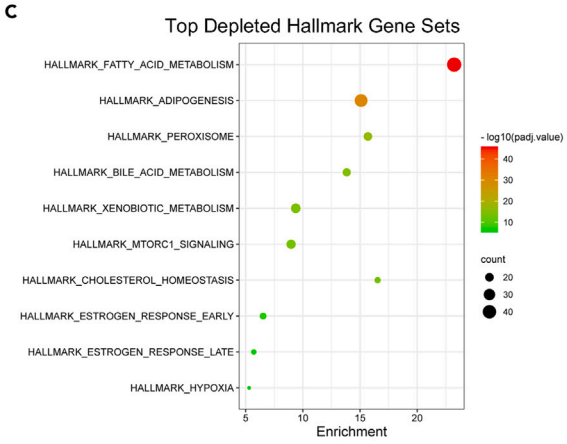
C
Top Depleted Hallmark Gene Sets
HALLMARK_FATTY_ACID_METABOLISM
HALLMARK_ADIPOGENESIS
HALLMARK_PEROXISOME
HALLMARK_BILE_ACID_METABOLISM
HALLMARK_XENOBIOTIC_METABOLISM
HALLMARK_MTORC1_SIGNALING
HALLMARK_CHOLESTEROL_HOMEOSTASIS
HALLMARK_ESTROGEN_RESPONSE_EARLY
HALLMARK_ESTROGEN_RESPONSE_LATE
HALLMARK_HYPOXIA
- log10(padj.value)
count
Enrichment

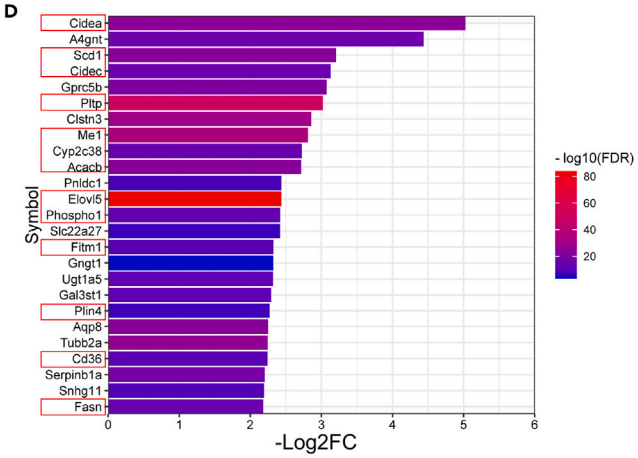
D
Cidea
A4gnt
Scd1
Cidec
Gprc5b
Pltp
Clstn3
Me1
Cyp2c38
Acacb
Pnldc1
Elovl5
Phospho1
Slc22a27
Fitm1
Gngt1
Ugt1a5
Gal3st1
Plin4
Aqp8
Tubb2a
Cd36
Serpinb1a
Snhg11
Fasn
Symbol
- log10(FDR)
-Log2FC

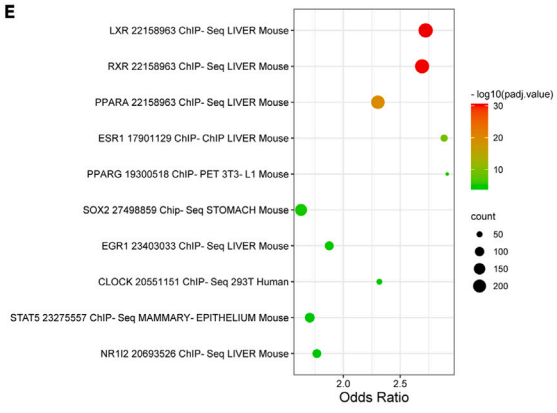
E
LXR 22158963 ChIP- Seq LIVER Mouse
RXR 22158963 ChIP- Seq LIVER Mouse
PPARA 22158963 ChIP- Seq LIVER Mouse
ESR1 17901129 ChIP- ChIP LIVER Mouse
PPARG 19300518 ChIP- PET 3T3- L1 Mouse
SOX2 27498859 Chip- Seq STOMACH Mouse
EGR1 23403033 ChIP- Seq LIVER Mouse
CLOCK 20551151 ChIP- Seq 293T Human
STAT5 23275557 ChIP- Seq MAMMARY- EPITHELIUM Mouse
NR1I2 20693526 ChIP- Seq LIVER Mouse
- log10(padj.value)
count
Odds Ratio

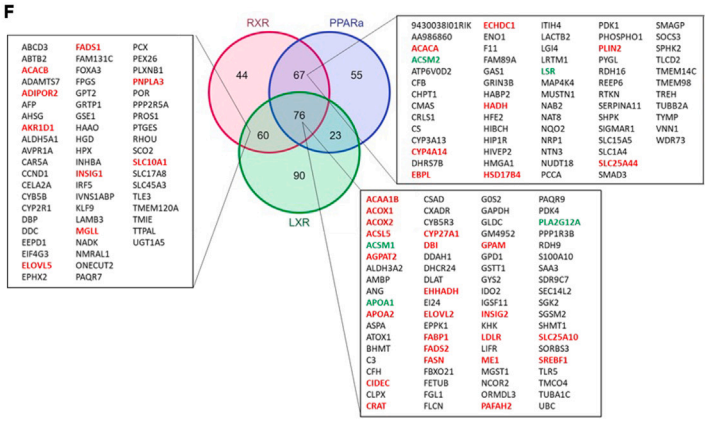
F
RXR
PPARa
LXR
44
67
55
76
60
23
90

**Figure 4. RNA-seq analysis reveals drastic metabolic remodeling in *Huwe1*$^{LKO}$ livers is recapitulated at the transcript level**

(A) Heatmap displaying differentially expressed genes between 1-year-old *Huwe1*$^{WT}$ and *Huwe1*$^{LKO}$ livers identified by RNA-seq.

(B) Volcano plot showing significantly upregulated (Red) and downregulated (Blue) genes in *Huwe1*$^{LKO}$ livers. Significance cutoffs set at |log2FC| > 0.5, padj <0.05.

(C) Hallmark gene set enrichment analysis performed on 618 significantly downregulated genes in *Huwe1*$^{LKO}$ livers. As observed in the mass spectrometry analysis (Figure 3C), "HALLMARK_FATTY_ACID_METABOLISM" was also the top downregulated gene set from *Huwe1*$^{LKO}$ livers identified by RNA-seq.

(D) Bar graph showing the top 25 depleted genes from *Huwe1*$^{LKO}$ livers sorted by -log2FC. Notably, many of these proteins were related to lipid metabolism or associated pathways (highlighted in red boxes).

(E and F) ChEA analysis on all 1,142 differentially expressed genes in *Huwe1*$^{LKO}$ livers identified by RNA-seq revealed strong enrichment of RXR, PPARα, and LXR activity (E). As observed in our mass spectrometry analysis, many of the differentially expressed genes in *Huwe1*$^{LKO}$ livers are predicted to be regulated by RXR, PPARα, and/or LXR (F). Upregulated (Green) and downregulated (Red) genes related to fatty acid metabolism are highlighted.

with LFD or HFD until they reached 1 year of age (Figure 6A). As seen in our diet study in 24-week-old mice, HFD promoted body weight gain in both genotypes relative to LFD-fed mice (Figure 6B). No differences were seen in the diet consumed between genotypes in both diet groups (Figure 6C). Additionally, a modest but statistically significant 6.5% reduction in body weight was observed in HFD-fed *Huwe1*$^{LKO}$ mice relative to *Huwe1*$^{WT}$ mice ($p = 0.01$; Figure 6B). Body composition analysis by EchoMRI revealed a significant increase in body fat percentage in *Huwe1*$^{WT}$ mice following HFD that was not observed in *Huwe1*$^{LKO}$ mice (Figure 6D). Conversely, this observation coincided with a significant decrease in lean mass percentage in HFD-fed *Huwe1*$^{WT}$ mice and no change in HFD-fed *Huwe1*$^{LKO}$ mice (Figure 6D). Although *Huwe1*$^{WT}$ mice exhibited marginally higher body fat percentage than *Huwe1*$^{LKO}$ mice before LFD/HFD administration (Figure 6E), no significant difference in body fat or lean mass percentage was observed between both 1-year-old LFD cohorts (Figure 6D). As seen in the 24-week-old mice (Figure 5D), HFD promoted the enlargement of subcutaneous iWAT fat pads in 1-year-old mice of both genotypes (Figure 6F). Notably, HFD-fed *Huwe1*$^{LKO}$ mice also exhibited a significant reduction in iWAT size relative to HFD-fed *Huwe1*$^{WT}$ mice, indicating protection against diet-induced obesity (Figure 6F). Again, no difference in the eWAT was observed between groups (Figure 6G). As seen in the 24-week-old mice, HFD induced the increased mass of iBAT in *Huwe1*$^{WT}$ mice but not *Huwe1*$^{LKO}$ mice (Figure 6H). These results demonstrate that the reduction in body weight in HFD-fed *Huwe1*$^{LKO}$ mice may be in part attributable to reduced subcutaneous fat accumulation but not increased thermogenesis.

We observed drastic differences in liver morphology in *Huwe1*$^{LKO}$ mice relative to *Huwe1*$^{WT}$ mice, with *Huwe1*$^{LKO}$ mice harboring noticeably healthier livers with a less mottled appearance (Figure 7A). Importantly, *Huwe1*$^{LKO}$ livers did not increase in size following HFD challenge and remained significantly smaller than HFD-fed *Huwe1*$^{WT}$ livers (Figure 7B). In addition, *Huwe1*$^{LKO}$ mice exhibit reduced levels of lipid droplets as compared to respective *Huwe1*$^{WT}$ diet groups (Figure 7C). *Huwe1*$^{LKO}$ livers also did not exhibit an increase in hepatic triglyceride content following HFD challenge, which remained significantly lower relative to HFD-fed *Huwe1*$^{WT}$ mice (Figure 7D). As expected, fecal triglyceride levels increased when the mice were on HFD (Figure 7E). However, there was no significant difference in the fecal triglyceride levels between *Huwe1*$^{WT}$ and HFD-fed *Huwe1*$^{LKO}$ mice (Figure 7E), indicating that reduced hepatic triglyceride content in *Huwe1*$^{LKO}$ mice is unlikely due to malabsorption of dietary fat.

Importantly, compared to LFD, HFD significantly induced *Cd36* expression, while downregulating *Fasn* expression in *Huwe1*$^{WT}$ livers (Figures 7F and 7G). However, this effect was not observed in *Huwe1*$^{LKO}$ livers (Figures 7F and 7G). In fact, the expression levels of both *Cd36* and *Fasn* remained attenuated in *Huwe1*$^{LKO}$ livers, regardless of the diets (Figures 7F and 7G). Advanced NAFLD is often associated with inflammation, cirrhosis, and fibrosis. We found that the expression of three pro-inflammatory immune cell markers (*Tnfa*, *Cxcl10*, and *Cd68*) was robustly increased in livers from HFD-fed *Huwe1*$^{WT}$ mice, compared to LFD-fed *Huwe1*$^{WT}$ mice (Figures 7H–7J). In contrast, this HFD-mediatedinduction of the immune cell markers was mitigated in *Huwe*$^{LKO}$ mice (Figures 7H–7J). Likewise, livers from HFD-fed *Huwe1*$^{WT}$ mice showed more F4/80 staining-positive macrophages than livers from HFD-fed *Huwe1*$^{LKO}$ mice (Figures 7K–7L). Sirius Red staining also revealed mild fibrosis in LFD-fed *Huwe1*$^{WT}$ mice which was largely absent in LFD-fed *Huwe*$^{LKO}$ mice (Figure S3 [*Huwe1*$^{LKO}$ livers exhibit reduced macrophage infiltration and fibrosis]). Notably, HFD-fed *Huwe*$^{LKO}$ mice were also protected against the HFD-induced fibrosis observed in *Huwe1*$^{WT}$ mice (Figure S3 [*Huwe1*$^{LKO}$ livers exhibit reduced macrophage infiltration and fibrosis]). Taken together, these results indicate that *Huwe1*$^{LKO}$ not only safeguards mice from age- and diet-induced NAFLD but also confers a mild degree of protection from inflammation and fibrosis.

NAFLD is often viewed as the hepatic manifestation of metabolic syndrome, a collection of disorders that include obesity, T2DM, dyslipidemia, cardiovascular disease, and insulin resistance.[26] As NAFLD almost universally presents with insulin resistance,[27] studies have shown that NAFLD often predates the development of T2DM.[28] Furthermore, obesity and T2DM have been proposed as major risk factors for progression of NAFLD to HCC.[29,30] Since a central metabolic function of the liver is regulating glucose availability,[31] we next investigated whether liver-specific *Huwe1* inactivation affected systemic glucose handling. At 24 weeks of age (prior to LFD/HFD diet administration) no significant differences were seen in the fasting blood glucose levels between groups (Figure 8A). After 28 weeks on LFD/HFD (Figure 6A), HFD 1-year-old *Huwe1*$^{WT}$ mice exhibited a significant increase in fasting blood glucose levels compared to LFD *Huwe1*$^{WT}$ mice while no change was observed in *Huwe1*$^{LKO}$ mice (Figure 8B). However, fasting glucose levels in 1-year-old HFD-fed *Huwe1*$^{LKO}$ mice were only modestly reduced as compared to HFD-fed *Huwe1*$^{WT}$ mice, with borderline statistical significance ($p = 0.087$). We then assessed the glucose clearing capability of these mice by performing glucose tolerance tests. Notably, *Huwe1*$^{LKO}$ mice exhibited improved glucose clearance compared to *Huwe1*$^{WT}$ mice even prior to LFD/HFD administration at 24-week age (Figure 8C). As diet- and age-induced NAFLD progressed in these mice, HFD-fed *Huwe1*$^{WT}$ mice demonstrated worsened glucose clearance kinetics as compared to LFD-fed *Huwe1*$^{WT}$ mice at 1 year of age (Figure 8D).

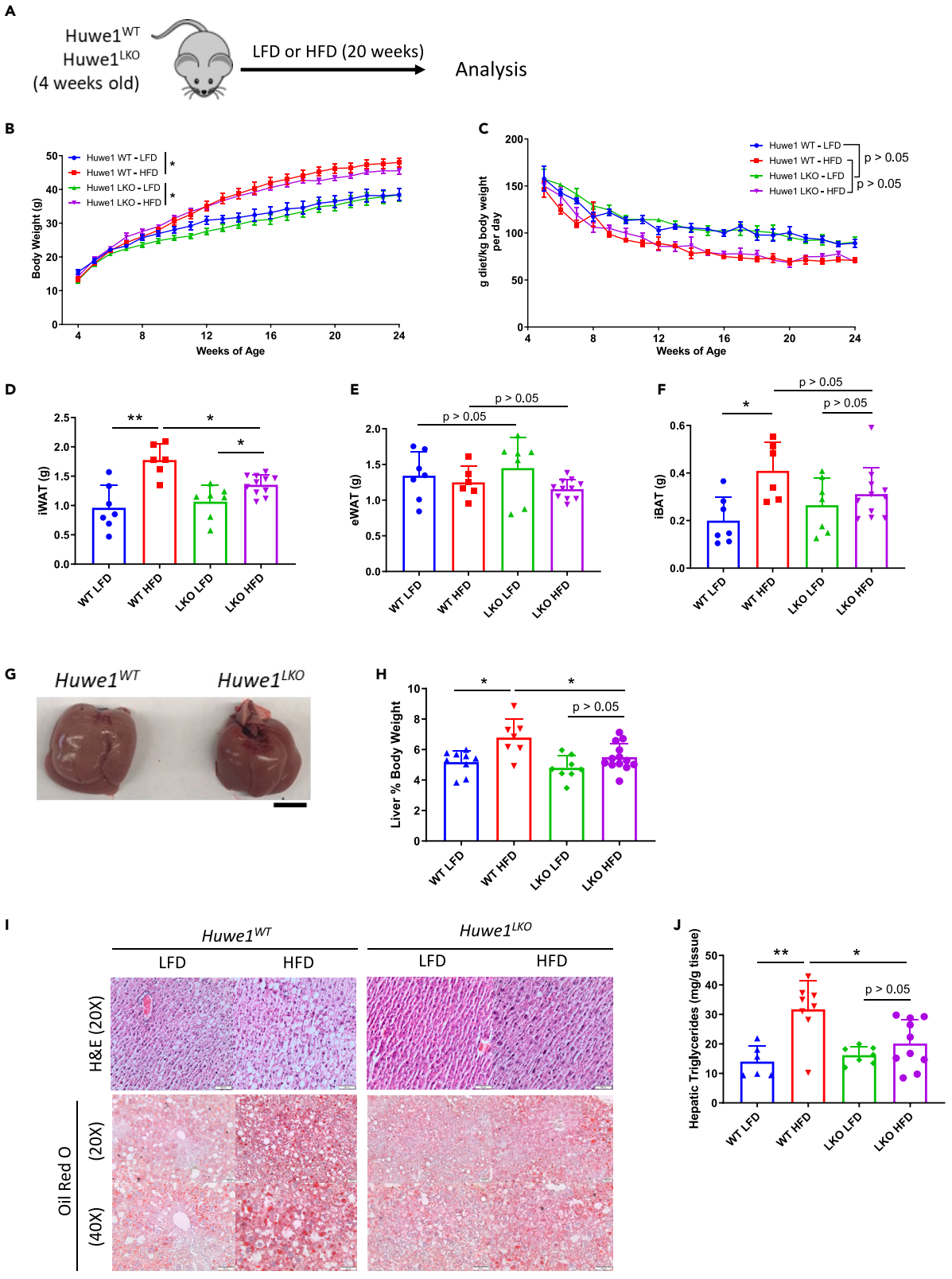
A
Huwe1WT
Huwe1LKO
(4 weeks old)
LFD or HFD (20 weeks)
Analysis
B
Huwe1 WT - LFD
Huwe1 WT - HFD
Huwe1 LKO - LFD
Huwe1 LKO - HFD
Body Weight (g)
Weeks of Age
C
g diet/kg body weight per day
p > 0.05
p > 0.05
Weeks of Age
D
iWAT (g)
WT LFD
WT HFD
LKO LFD
LKO HFD
E
eWAT (g)
p > 0.05
p > 0.05
F
iBAT (g)
p > 0.05
p > 0.05
G
Huwe1WT
Huwe1LKO
H
Liver % Body Weight
p > 0.05
I
Huwe1WT
Huwe1LKO
LFD
HFD
H&E (20X)
Oil Red O
(20X)
(40X)
J
Hepatic Triglycerides (mg/g tissue)
p > 0.05

**Figure 5. Young *Huwe1*$^{LKO}$ mice are protected from HFD-induced hepatic steatosis but not body weight gain**

(A) 4-week-old *Huwe1*$^{WT}$ and *Huwe1*$^{LKO}$ were challenged with LFD or HFD for 20 weeks. N = 10–16 mice per group.

(B and C) Body weight gain (B) and diet consumption (C) of the mice over the course of the diet study. *Huwe1*$^{WT}$ and *Huwe1*$^{LKO}$ exhibited no difference in diet consumed and both gained a nearly equal amount of weight following HFD. Data are shown as mean ± SEM. See STAR Methods section for further detail of growth curve analysis.

(D–F) Weight of iWAT (D), eWAT (E), and iBAT (F) from the mice following 20 weeks of LFD or HFD.

(G) Representative pictures of *Huwe1*$^{WT}$ and *Huwe1*$^{LKO}$ mice challenged with HFD. Scale bar represents 1 cm.

(H) Liver weight normalized to body weight.

(I) H&E and ORO stains showed reduced lipid droplet accumulation in *Huwe1*$^{LKO}$ livers following HFD as compared to *Huwe1*$^{WT}$ livers.

(J) Biochemical analysis measuring hepatic triglyceride levels. Data shown as mean +SD. Significance assessed by two-sided Student's *t* test with significance set at * <0.05, ** <0.005.

Importantly, *Huwe1*$^{LKO}$ mice showed marked resistance to developing diet-induced glucose intolerance as HFD-fed *Huwe1*$^{LKO}$ mice demonstrated no change in glucose clearing capability (Figure 8D).

Lastly, we observed that spontaneous liver tumors developed in 2 out of 12 HFD-fed 1-year-old *Huwe1*$^{WT}$ mice but not in *Huwe1*$^{LKO}$ mice (Figure 8E). No tumors were observed in either of the 1-year-old LFD groups (Figure 8E). Additionally, no tumors were observed in any of the young LFD/HFD-fed mice (Figure 5A), indicating that aging plays a key role in the etiology of these lesions. These findings collectively demonstrate that 1-year-old *Huwe1*$^{LKO}$ mice remain markedly protected against HFD-induced obesity, hepatic steatosis, glucose intolerance, and incidence of HCC (Figure 8F).

## DISCUSSION

Hepatic steatosis results from an imbalance of lipid homeostatic processes such as FA acquisition through extracellular uptake or *de novo* synthesis, elimination through β-oxidation or storage in triglycerides, as well as secretion into the circulation in the form of lipoproteins.[32] In the current study, we demonstrated that liver-specific deletion of *Huwe1* resulted in significant remodeling of several lipid metabolism pathways, including attenuation of *de novo* lipogenesis, FA uptake, and peroxisomal FA β-oxidation, as well as increased mitochondrial FA β-oxidation and oxidative phosphorylation (Figures 3C–3E, 4C, and 4D). Notably, downregulation of FA synthesis genes in *Huwe1*$^{LKO}$ livers was concordant at both protein and mRNA levels (Figures 3D and 4D), suggesting that this alteration likely originates at the transcriptional level. Indeed, ChEA analysis revealed that the dysregulation of lipid metabolism genes in 1-year-old *Huwe1*$^{LKO}$ livers was, at least in part, secondary to the attenuated activity of the 3 major hepatic transcription factors: LXR, RXR, and PPARα (Figures 3F and 4E). Interestingly, modestly diminished protein expression of RXRα, the obligate dimeric partner of LXR and PPARα, was seen in 1-year-old *Huwe1*$^{LKO}$ livers (Figure 3H). Further study will be required to directly implicate the relationship between these specific transcription factors and their unique subset of targets following inactivation of *Huwe1*. In contrast, upregulation of several components of the mitochondrial β-oxidation pathway in *Huwe1*$^{LKO}$ livers was observed strictly at protein levels, suggesting that this alteration is likely a result of protein stabilization (Figures S1A and S1B [*Huwe1*$^{LKO}$ livers from 1-year-old mice exhibit enrichment of metabolic proteins and pathways]; Table S1 [Significantly enriched proteins in *Huwe1*$^{LKO}$ livers]). Since Huwe1 is an E3 ubiquitin ligase, it is tempting to speculate that at least some of the proteins involved in mitochondrial β-oxidation might be direct substrates of Huwe1, although this needs to be experimentally validated. All in all, our results strongly suggest that the downregulation of *de novo* lipogenesis and FA uptake together with the upregulation of the mitochondrial β-oxidation pathways underlies the ameliorated lipid accumulation phenotype observed in the *Huwe1*$^{LKO}$ mice (Figure 8F).

Previously, studies in human NAFLD and NASH patients have demonstrated that hepatic expression of the FA transporter CD36 increases with the development of NASH and is significantly associated with elevated plasma insulin levels, insulin resistance, and histologic grade of steatosis.[33,34] Additionally, the expression of *de novo* lipogenesis genes is also known to be essential for the development of hepatic steatosis.[35] We identified *Cd36* and several lipogenic genes (e.g., *Srebf1*, *Acly*, *Acaca*, *Fasn*, and *Scd*) to be among the most downregulated in *Huwe1*$^{LKO}$ mouse livers by mass spectrometry and RNA-seq (Table S2 [Significantly depleted proteins in *Huwe1*$^{LKO}$ livers]; Table S5 [Significantly depleted mRNA transcripts in *Huwe1*$^{LKO}$ livers]; Figures 3D and 4D). Importantly, many of these genes, including *Cd36*, are regulated by LXR, RXR, and/or PPARα,[23,36,37] consistent with our ChEA analysis (Figures 3G and 4E). It should be noted that PPARα (as well as RXR and LXR) requires ligand binding (FA derivatives for PPARα-RXR and cholesterol derivatives for LXR-RXR) for its full activation.[23] Given the low levels of triglycerides in *Huwe1*$^{LKO}$ mouse livers, it is possible that the reduced expression of PPARα, RXR, and LXR-target genes may also be attributable in part due to the lack of available ligands to activate these transcription factors. Interestingly, a recent study has shown that Huwe1 promotes the degradation of PPARα through the progestin and adipoQ receptor 3 (PAQR3)-mediated pathway,[38] which somewhat contradicts our results (Figures 3G and 4E). However, other E3 ligases were also found to co-immunoprecipitate with PPARα[38], albeit with lower abundance than Huwe1. We hypothesize that PAQR3 recruits a different E3 ligase in *Huwe1*$^{LKO}$ livers to facilitate PPARα degradation and that this is why *Huwe1* inactivation does not affect PPARα protein levels in our model.

In addition to preventing aberrant hepatic lipid accumulation, *Huwe1*$^{LKO}$ also confers protection against the development of HFD-induced glucose intolerance (Figure 8). We find that *Huwe1* inactivation in the liver improves glucose clearance in mice by 24 weeks of age (Figure 8C) and protects against glucose intolerance induced by HFD in 1-year-old mice (Figure 8D). Notably, it was previously shown that pancreatic β-cell-specific *Huwe1* knockout resulted in a progressive hyperglycemia and diabetic phenotype due to p53 activation and cell death of islet cells.[15] Therefore, this study further emphasizes that the role of Huwe1 *in vivo* is often context dependent and may vary between tissues. Huwe1 is a well-established negative regulator of the tumor suppressor p53.[5] Although most widely studied for its anti-tumorigenic

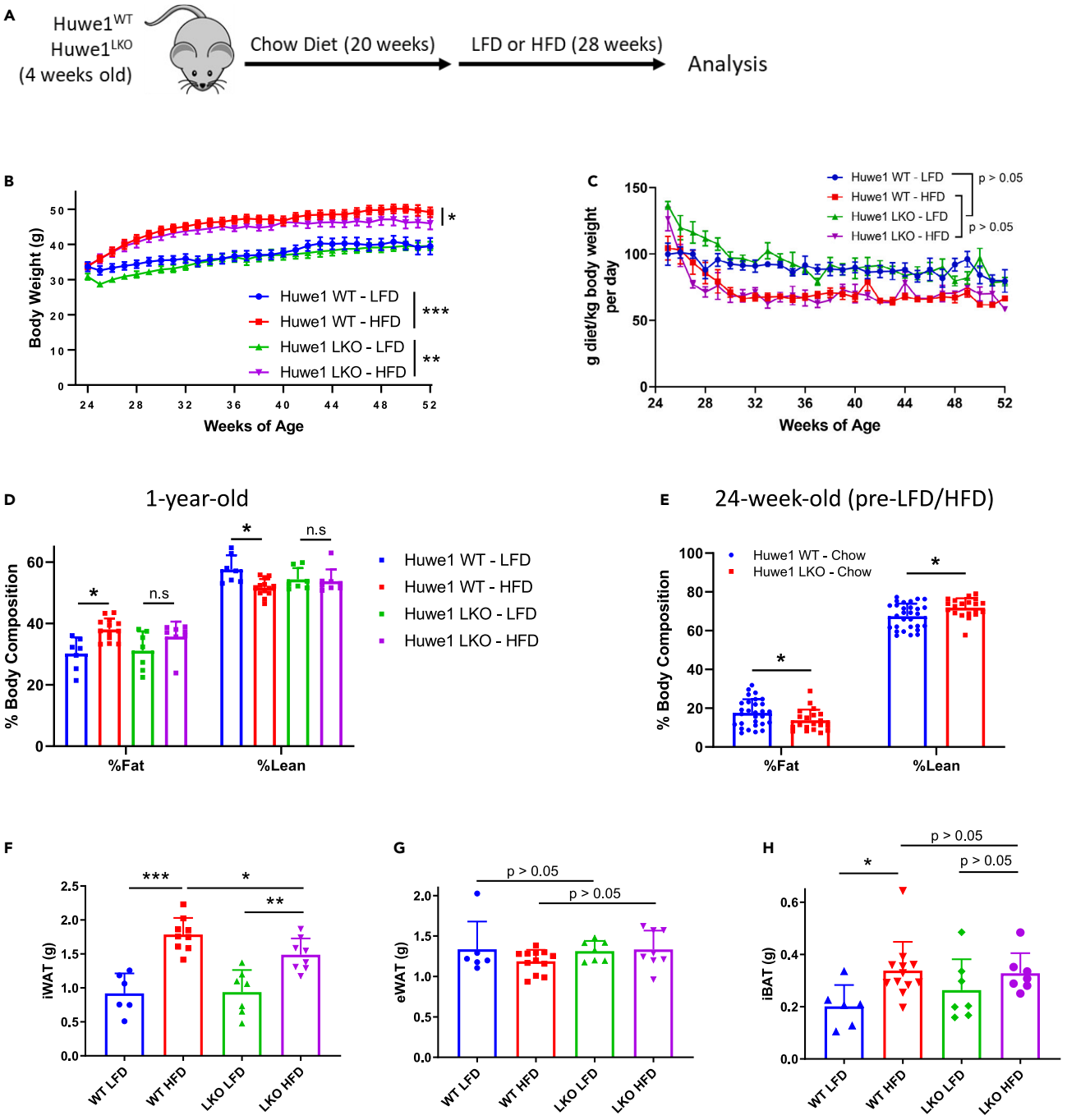


**Figure 6. Aged *Huwe1*$^{LKO}$ mice are protected against HFD-induced obesity**

(A) 24-week-old *Huwe1*$^{WT}$ and *Huwe1*$^{LKO}$ raised on chow diet were challenged with LFD or HFD for 28 weeks until mice reached 1 year of age. N = 8–15 mice per diet group.

(B and C) Body weight gain (B) and diet consumption (C) of the mice over the course of the diet study. Despite no differences in diet consumption, HFD-fed *Huwe1*$^{LKO}$ mice exhibited a modest reduction in body weight accumulation as compared to HFD-fed *Huwe1*$^{WT}$ mice. Data are shown as mean ± SEM. See STAR Methods section for further detail of growth curve analysis.

(D and E) Body composition was measured using EchoMRI on 1-year-old mice after LFD/HFD challenge (D) as well as at 24 weeks before randomization (E).

(F–H) Weight of iWAT (F), eWAT (G), and iBAT (H) from the mice following 28 weeks of LFD or HFD. Unless otherwise specified, the data are shown in this figure as mean +SD with significance assessed by two-sided Student's *t* test with significance set at * <0.05, ** <0.005.

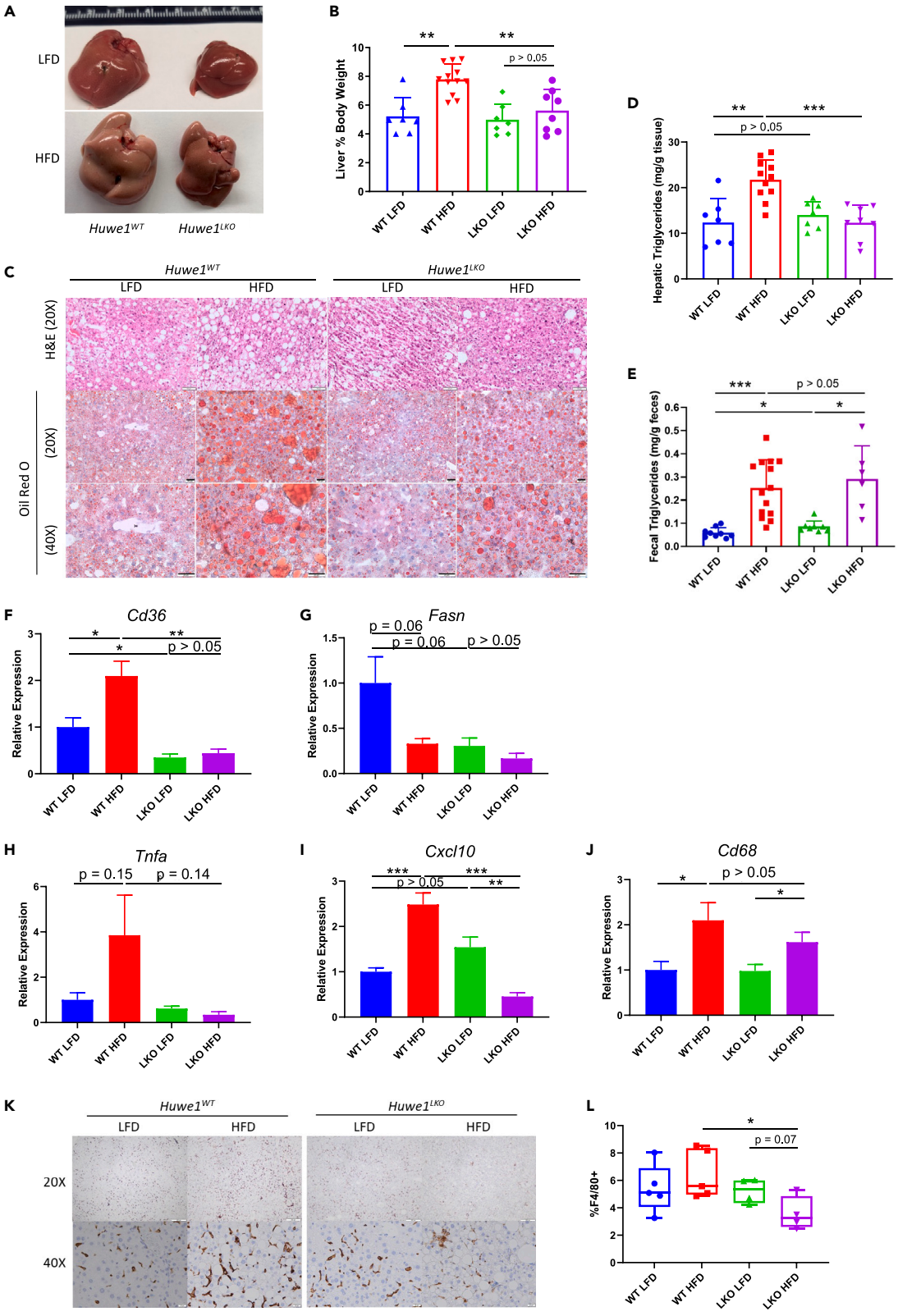
A
LFD
HFD
Huwe1WT
Huwe1LKO
B
Liver % Body Weight
**
**
p > 0.05
WT LFD
WT HFD
LKO LFD
LKO HFD
C
Huwe1WT
Huwe1LKO
LFD
HFD
H&E (20X)
Oil Red O
(20X)
(40X)
D
Hepatic Triglycerides (mg/g tissue)
**
***
p > 0.05
E
Fecal Triglycerides (mg/g feces)
***
p > 0.05
*
F
Cd36
Relative Expression
G
Fasn
p = 0.06
p = 0.06
p > 0.05
H
Tnfa
p = 0.15
p = 0.14
I
Cxcl10
J
Cd68
K
20X
40X
L
%F4/80+
p = 0.07

**Figure 7. Aged *Huwe1*$^{LKO}$ mice are protected against HFD-induced NAFLD**

(A) Representative images of livers collected from 1-year-old *Huwe1*$^{WT}$ and *Huwe1*$^{LKO}$ mice maintained on LFD/HFD.

(B) Liver weight normalized to body weight.

(C) H&E and ORO stains showed reduced lipid droplet accumulation in *Huwe1*$^{LKO}$ livers following HFD as compared to *Huwe1*$^{WT}$ livers.

(D and E) Biochemical analysis measuring hepatic (D) and fecal (E) triglyceride levels.

(F–J) RT-qPCR analysis on liver samples reveals attenuated expression of *Cd36*, *Fasn*, and pro-inflammatory cytokines in *Huwe1*$^{LKO}$ livers following HFD as compared to *Huwe1*$^{WT}$.

(K–L) IHC staining for F4/80 shows reduced macrophage infiltration in *Huwe1*$^{LKO}$ mice challenged with HFD as compared to *Huwe1*$^{WT}$ mice (K). Box and whisker plot depicting quantification of %F4/80+ area (L). Data shown as mean +SD (B, D, andE) or SEM (F–J). Significance assessed by two-sided Student's *t* test with significance set at * <0.05, ** <0.005, *** <0.0005.

properties, p53 is also well known to exert functions in regulating various aspects of metabolism including lipid homeostasis, glycolysis, and insulin resistance.[39–41] In response to perturbations in nutrient availability, ribosomal stress and ribosomal protein-mediated degradation of MDM2, the major negative regulator of p53, have been shown to mediate the activation of p53.[39,42] It was recently demonstrated that HFD induces p53 in a c-MYC- and RPL11-dependent fashion in wild-type mice but not in global knockin mice bearing a single amino acid substitution in MDM2 (C305F).[39] The defect in p53 activation observed in C305F HFD-challenged mice was associated with a reduction in hepatic triglyceride content and improved glucose tolerance, analogous to what we observe in our HFD-fed *Huwe1*$^{LKO}$ mice.[39] Notably, the phenotype observed in C305F mice was attributable to RPL11-MDM2-p53 signaling specifically in adipose tissue but not the liver, since no differences were observed in hepatic levels of RPL11, p53, or the p53 target gene p21 in C305F mice.[39] These results suggest that the role of RPL11-MDM2-p53 axis on the maintenance of lipid homeostasis may be tissue-specific and dispensable in the context of liver biology. As such, because no differences in p53 or p53 target genes were observed in *Huwe1*$^{LKO}$ mice from the current study (Figure S2C [*Huwe1*$^{LKO}$ livers from 1-year-old mice do not exhibit enrichment of lipid metabolic genes and pathways]), the protection from NAFLD observed in *Huwe1*$^{LKO}$ mice appears to arise independent of p53 signaling.

While the biggest functional effects of *Huwe1* deletion are seen in 1-year-old mice challenged with HFD, aspects of this protective phenotype begin to manifest earlier in life. For example, despite exhibiting no difference in liver size at 24 weeks of age (Figure 2B), *Huwe1*$^{LKO}$ mice on chow diet already demonstrate reduced body fat accumulation (Figure 6E) and improved glucose tolerance (Figure 8C). Therefore, the protective effects observed in HFD-fed 1-year-old *Huwe1*$^{LKO}$ mice may accumulate over the entire lifespan. Importantly, although hepatic steatosis is reversible in early NAFLD, liver damage resulting from inflammation, cirrhosis, and fibrosis observed in advanced stages are often irreversible and predispose individuals to HCC.[4,29] Outside of diet and exercise, treatment strategies for NAFLD remain limited as there are no FDA-approved pharmaceutical options available. Ultimately, our study identifies Huwe1 as a potentially valuable therapeutic target for NAFLD prevention.

## STAR★METHODS

Detailed methods are provided in the online version of this paper and include the following:

- KEY RESOURCES TABLE
- RESOURCE AVAILABILITY
  - Lead contact
  - Materials availability
  - Data and code availability
- EXPERIMENTAL MODEL AND STUDY PARTICIPANT DETAILS
  - Mice
- METHOD DETAILS
  - Glucose tolerance test
  - Immunohistochemistry (IHC)
  - ORO staining
  - Triglyceride and cholesterol quantification
  - RNA-seq
  - Real-time quantitative PCR (RT-qPCR)
  - Western blot
  - Sample preparation for proteomics analysis
  - LC-MS/MS analysis
  - Statistical analysis

## SUPPLEMENTAL INFORMATION

Supplemental information can be found online at https://doi.org/10.1016/j.isci.2023.108405.

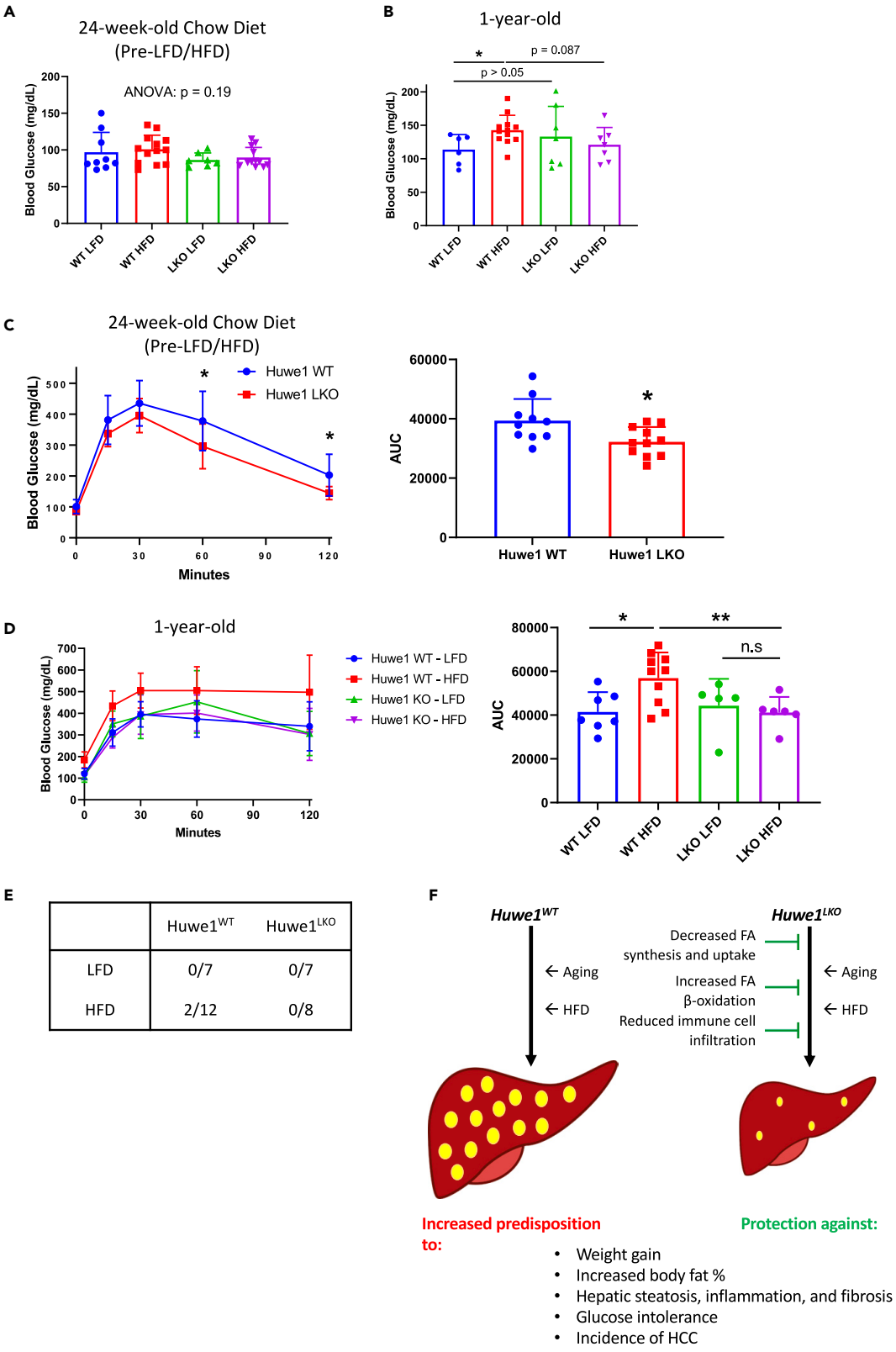


| | Huwe1$^{WT}$ | Huwe1$^{LKO}$ |
|---|---|---|
| LFD | 0/7 | 0/7 |
| HFD | 2/12 | 0/8 |

**Figure 8. Aged *Huwe1*$^{LKO}$ mice are protected against HFD-induced glucose intolerance**

(A) Fasting blood glucose levels of 24-week-old *Huwe1*$^{WT}$ and *Huwe1*$^{LKO}$ mice raised on chow diet before enrollment into LFD/HFD-challenge arms.

(B) Fasting blood glucose levels of 1-year-old *Huwe1*$^{WT}$ and *Huwe1*$^{LKO}$ mice raised on LFD/HFD. Data shown as mean +SD. Statistical significance measured using one-way ANOVA (A) or two-sided Student's *t* test with significance set at * <0.05 (B).

(C and D) Glucose tolerance test run on fasted 24-week-old *Huwe1*$^{WT}$ and *Huwe1*$^{LKO}$ mice raised on chow diet (C) and 1-year-old LFD/HFD-challenged mice (D).

(E) Aged *Huwe1*$^{LKO}$ mice exhibit reduced incidence of spontaneous HCC following HFD challenge as compared to *Huwe1*$^{WT}$ mice.

(F) Our proposed model of how liver-specific *Huwe1* inactivation protects against hepatic steatosis and glucose intolerance induced by aging and/or HFD. Unless otherwise specific, the data in this figure are shown as mean +SD with statistical significance assessed by two-sided Student's *t* test with significance set at * <0.05, ** <0.005, *** <0.0005.

## ACKNOWLEDGMENTS

We would like to thank Sandeep Kaur, Rebecca Brady, Peighton Neuman, Andrew Whitfield, Grace Jones, and Harley Moser for their assistance with the animal work. We would also like to thank Jessica Ferrell, Yanqiao Zhang, John Chiang, Liya Yin, Yoon-Kwang Lee, Shannon Boehme, and Sharon Usip at Northeast Ohio Medical University for the valuable discussion and suggestion as well as their assistance with histology. This study was supported by an NIH R15 DK121246, an NIH R15 DK108668 (to C.M.N.), an NIH Career Development Award R00 CA140948, an NIH R03 CA230828, an NIH R15 CA256838, and an NIH R21 AG081896-01 (to M.K.). E.M.T. was a SURE program scholar and a Student Research Experience (SRE) Scholar at Kent State University. E.M.T. was also a recipient of the Ralph W. Dexter Faculty Award at Kent State University. We dedicate this paper to the memory of Professor Derek Damron at Kent State University. The graphical abstract was created with BioRender.com. Finally, we thank the support from the Department of Biological Sciences at Kent State Univerasity.

## AUTHOR CONTRIBUTIONS

Conception and Design, W.W.F. and M.K.; Development of Methodology, W.W.F., S.B., and E.M.T.; Acquisition of Data, W.W.F., S.B., E.M.T., C.D., K.J.C., R.A.-S., D.B.A., W.W., S.I., and T.K.; Analysis and Interpretation of Data, W.W.F., S.B., E.M.T., R.A.-S., D.B.A., W.W., S.I., T.K., and M.K.; Writing of the Manuscript; W.W.F., E.M.T., T.K., and M.K.; Administrative, Technical, or Material Support, W.W., S.I., T.K., N.K., W.G., and C.M.N.; Study Supervision: M.K.

## DECLARATION OF INTERESTS

The authors declare no competing interests.

## INCLUSION AND DIVERSITY

We support inclusive, diverse, and equitable conduct of research.

Received: January 6, 2023
Revised: September 3, 2023
Accepted: November 3, 2023
Published: November 7, 2023

## REFERENCES

1. Rinella, M.E. (2015). Nonalcoholic fatty liver disease: a systematic review. JAMA *313*, 2263–2273.
2. Brunt, E.M. (2010). Pathology of nonalcoholic fatty liver disease. Nat. Rev. Gastroenterol. Hepatol. *7*, 195–203.
3. Baffy, G., Brunt, E.M., and Caldwell, S.H. (2012). Hepatocellular carcinoma in non-alcoholic fatty liver disease: An emerging menace. J. Hepatol. *56*, 1384–1391.
4. Sheedfar, F., Di Biase, S., Koonen, D., and Vinciguerra, M. (2013). Liver diseases and aging: friends or foes? Aging Cell *12*, 950–954.
5. Chen, D., Kon, N., Li, M., Zhang, W., Qin, J., and Gu, W. (2005). ARF-BP1/Mule is a critical mediator of the ARF tumor suppressor. Cell *121*, 1071–1083.
6. Adhikary, S., Marinoni, F., Hock, A., Hulleman, E., Popov, N., Beier, R., Bernard, S., Quarto, M., Capra, M., Goettig, S., et al. (2005). The ubiquitin ligase HectH9 regulates transcriptional activation by Myc and is essential for tumor cell proliferation. Cell *123*, 409–421.
7. Zhong, Q., Gao, W., Du, F., and Wang, X. (2005). Mule/ARF-BP1, a BH3-only E3 ubiquitin ligase, catalyzes the polyubiquitination of Mcl-1 and regulates apoptosis. Cell *121*, 1085–1095.
8. Zhao, X., Heng, J.I.T., Guardavaccaro, D., Jiang, R., Pagano, M., Guillemot, F., Iavarone, A., and Lasorella, A. (2008). The HECT-domain ubiquitin ligase Huwe1 controls neural differentiation and proliferation by destabilizing the N-Myc oncoprotein. Nat. Cell Biol. *10*, 643–653.
9. Zhao, X., D' Arca, D., Lim, W.K., Brahmachary, M., Carro, M.S., Ludwig, T., Cardo, C.C., Guillemot, F., Aldape, K., Califano, A., et al. (2009). The N-Myc-DLL3 cascade is suppressed by the ubiquitin ligase Huwe1 to inhibit proliferation and promote neurogenesis in the developing brain. Dev. Cell *17*, 210–221.
10. King, B., Boccalatte, F., Moran-Crusio, K., Wolf, E., Wang, J., Kayembe, C., Lazaris, C., Yu, X., Aranda-Orgilles, B., Lasorella, A., and Aifantis, I. (2016). The ubiquitin ligase Huwe1 regulates the maintenance and lymphoid commitment of hematopoietic stem cells. Nat. Immunol. *17*, 1312–1321.
11. Liu, Z., Oughtred, R., and Wing, S.S. (2005). Characterization of E3Histone, a novel testis ubiquitin protein ligase which ubiquitinates histones. Mol. Cell Biol. *25*, 2819–2831.
12. Bose, R., Sheng, K., Moawad, A.R., Manku, G., O'Flaherty, C., Taketo, T., Culty, M., Fok, K.L., and Wing, S.S. (2017). Ubiquitin ligase Huwe1 modulates spermatogenesis by regulating spermatogonial differentiation and entry into meiosis. Sci. Rep. *7*, 17759.
13. Fok, K.L., Bose, R., Sheng, K., Chang, C.-W., Katz-Egorov, M., Culty, M., Su, S., Yang, M., Ruan, Y.C., Chan, H.-C., et al. (2017). Huwe1 regulates the establishment and maintenance of spermatogonia by suppressing DNA damage response. Endocrinology *158*, 4000–4016.
14. Eisa, A.A., Bang, S., Crawford, K.J., Murphy, E.M., Feng, W.W., Dey, S., Wells, W., Kon, N.,

Gu, W., Mehlmann, L.M., et al. (2020). X-linked Huwe1 is essential for oocyte maturation and preimplantation embryo development. iScience *23*, 101523.
15. Kon, N., Zhong, J., Qiang, L., Accili, D., and Gu, W. (2012). Inactivation of arf-bp1 induces p53 activation and diabetic phenotypes in mice. J. Biol. Chem. *287*, 5102–5111.
16. Postic, C., Shiota, M., Niswender, K.D., Jetton, T.L., Chen, Y., Moates, J.M., Shelton, K.D., Lindner, J., Cherrington, A.D., and Magnuson, M.A. (1999). Dual roles for glucokinase in glucose homeostasis as determined by liver and pancreatic β cell-specific gene knock-outs using Cre recombinase. J. Biol. Chem. *274*, 305–315.
17. Flurkey, K., Currer, J.M., and Harrison, D.E. (2007). Mouse models in aging research. In The mouse in biomedical research (Academic Press), pp. 637–672.
18. Lonardo, A., Lombardini, S., Scaglioni, F., Ballestri, S., Verrone, A.M., Bertolotti, M., Carulli, L., Ganazzi, D., Carulli, N., and Loria, P. (2006). Fatty liver, carotid disease and gallstones: a study of age-related associations. World J. Gastroenterol. *12*, 5826–5833.
19. Zhang, X., Zhang, Y.-L., Qiu, G., Pian, L., Guo, L., Cao, H., Liu, J., Zhao, Y., Li, X., Xu, Z., et al. (2020). Hepatic neddylation targets and stabilizes electron transfer flavoproteins to facilitate fatty acid β-oxidation. Proc. Natl. Acad. Sci. USA *117*, 2473–2483.
20. Kuleshov, M.V., Jones, M.R., Rouillard, A.D., Fernandez, N.F., Duan, Q., Wang, Z., Koplev, S., Jenkins, S.L., Jagodnik, K.M., Lachmann, A., et al. (2016). Enrichr: a comprehensive gene set enrichment analysis web server 2016 update. Nucleic Acids Res. *44*, W90–W97.
21. Vogel, M.J., Peric-Hupkes, D., and van Steensel, B. (2007). Detection of in vivo protein–DNA interactions using DamID in mammalian cells. Nat. Protoc. *2*, 1467–1478.
22. Lachmann, A., Xu, H., Krishnan, J., Berger, S.I., Mazloom, A.R., and Ma'ayan, A. (2010). ChEA: transcription factor regulation inferred from integrating genome-wide ChIP-X experiments. Bioinformatics *26*, 2438–2444.
23. Wang, B., and Tontonoz, P. (2018). Liver X receptors in lipid signalling and membrane homeostasis. Nat. Rev. Endocrinol. *14*, 452–463.
24. Bardot, O., Aldridge, T.C., Latruffe, N., and Green, S. (1993). PPAR-RXR heterodimer activates a peroxisome proliferator response element upstream of the bifunctional enzyme gene. Biochem. Biophys. Res. Commun. *192*, 37–45.
25. Frith, J., Day, C.P., Henderson, E., Burt, A.D., and Newton, J.L. (2009). Non-alcoholic fatty liver disease in older people. Gerontology *55*, 607–613.
26. Kotronen, A., and Yki-Järvinen, H. (2008). Fatty liver: a novel component of the metabolic syndrome. Arterioscler. Thromb. Vasc. Biol. *28*, 27–38.
27. Tilg, H., Moschen, A.R., and Roden, M. (2017). NAFLD and diabetes mellitus. Nat. Rev. Gastroenterol. Hepatol. *14*, 32–42.
28. Marchesini, G., Brizi, M., Morselli-Labate, A.M., Bianchi, G., Bugianesi, E., McCullough, A.J., Forlani, G., and Melchionda, N. (1999). Association of nonalcoholic fatty liver disease with insulin resistance. Am. J. Med. *107*, 450–455.
29. El–Serag, H.B., and Rudolph, K.L. (2007). Hepatocellular carcinoma: epidemiology and molecular carcinogenesis. Gastroenterology *132*, 2557–2576.
30. Yasui, K., Hashimoto, E., Komorizono, Y., Koike, K., Arii, S., Imai, Y., Shima, T., Kanbara, Y., Saibara, T., Mori, T., et al. (2011). Characteristics of patients with nonalcoholic steatohepatitis who develop hepatocellular carcinoma. Clin. Gastroenterol. Hepatol. *9*, 428–433. quiz e50.
31. Han, H.-S., Kang, G., Kim, J.S., Choi, B.H., and Koo, S.-H. (2016). Regulation of glucose metabolism from a liver-centric perspective. Exp. Mol. Med. *48*, e218.
32. Jou, J., Choi, S.S., and Diehl, A.M. (2008). Mechanisms of disease progression in nonalcoholic fatty liver disease. Semin. Liver Dis. *28*, 370–379.
33. Sheedfar, F., Sung, M.M., Aparicio-Vergara, M., Kloosterhuis, N.J., Miquilena-Colina, M.E., Vargas-Castrillón, J., Febbraio, M., Jacobs, R.L., de Bruin, A., Vinciguerra, M., et al. (2014). Increased hepatic CD36 expression with age is associated with enhanced susceptibility to nonalcoholic fatty liver disease. Aging *6*, 281–295.
34. Miquilena-Colina, M.E., Lima-Cabello, E., Sánchez-Campos, S., García-Mediavilla, M.V., Fernández-Bermejo, M., Lozano-Rodríguez, T., Vargas-Castrillón, J., Buqué, X., Ochoa, B., Aspichueta, P., et al. (2011). Hepatic fatty acid translocase CD36 upregulation is associated with insulin resistance, hyperinsulinaemia and increased steatosis in non-alcoholic steatohepatitis and chronic hepatitis C. Gut *60*, 1394–1402.
35. Shimomura, I., Bashmakov, Y., and Horton, J.D. (1999). Increased levels of nuclear SREBP-1c associated with fatty livers in two mouse models of diabetes mellitus. J. Biol. Chem. *274*, 30028–30032.
36. Cave, M.C., Clair, H.B., Hardesty, J.E., Falkner, K.C., Feng, W., Clark, B.J., Sidey, J., Shi, H., Aqel, B.A., McClain, C.J., and Prough, R.A. (2016). Nuclear receptors and nonalcoholic fatty liver disease. Biochim. Biophys. Acta *1859*, 1083–1099.
37. Nakamura, M.T., Yudell, B.E., and Loor, J.J. (2014). Regulation of energy metabolism by long-chain fatty acids. Prog. Lipid Res. *53*, 124–144.
38. Zhao, Z., Xu, D., Wang, Z., Wang, L., Han, R., Wang, Z., Liao, L., and Chen, Y. (2018). Hepatic PPARα function is controlled by polyubiquitination and proteasome-mediated degradation through the coordinated actions of PAQR3 and HUWE1. Hepatology *68*, 289–303.
39. Liu, S., Kim, T.-H., Franklin, D.A., and Zhang, Y. (2017). Protection against high-fat-diet-induced obesity in $MDM2^{C305F}$ mice due to reduced p53 activity and enhanced energy expenditure. Cell Rep. *18*, 1005–1018.
40. Jiang, P., Du, W., Wang, X., Mancuso, A., Gao, X., Wu, M., and Yang, X. (2011). p53 regulates biosynthesis through direct inactivation of glucose-6-phosphate dehydrogenase. Nat. Cell Biol. *13*, 310–316.
41. Minamino, T., Orimo, M., Shimizu, I., Kunieda, T., Yokoyama, M., Ito, T., Nojima, A., Nabetani, A., Oike, Y., Matsubara, H., et al. (2009). A crucial role for adipose tissue p53 in the regulation of insulin resistance. Nat. Med. *15*, 1082–1087.
42. Liu, Y., He, Y., Jin, A., Tikunov, A.P., Zhou, L., Tollini, L.A., Leslie, P., Kim, T.-H., Li, L.O., Coleman, R.A., et al. (2014). Ribosomal protein–Mdm2–p53 pathway coordinates nutrient stress with lipid metabolism by regulating MCD and promoting fatty acid oxidation. Proc. Natl. Acad. Sci. USA *111*, E2414–E2422.
43. Ferrell, J.M., Boehme, S., Li, F., and Chiang, J.Y.L. (2016). Cholesterol 7α-hydroxylase-deficient mice are protected from high-fat/high-cholesterol diet-induced metabolic disorders. J. Lipid Res. *57*, 1144–1154.
44. Feng, W.W., Wilkins, O., Bang, S., Ung, M., Li, J., An, J., Del Genio, C., Canfield, K., DiRenzo, J., Wells, W., et al. (2019). CD36-mediated metabolic rewiring of breast cancer cells promotes resistance to HER2-targeted therapies. Cell Rep. *29*, 3405–3420.e5.

## STAR★METHODS

### KEY RESOURCES TABLE

| REAGENT or RESOURCE | SOURCE | IDENTIFIER |
|---|---|---|
| Antibodies | | |
| Rabbit polyclonal anti-Huwe1 | Bethyl Laboratories | Cat # A300-486A; RRID:AB_2264590 |
| Mouse monoclonal anti-beta-Actin | Santa Cruz Biotechnology | Cat # SC-69879; RRID:AB_1119529 |
| Mouse monoclonal anti-FASN | BD Biosciences | Cat # 610962; RRID:AB_398275 |
| Goat polyclonal anti-CD36 | R&D Systems | Cat # AF2519; RRID:AB_2228767 |
| Rabbit polyclonal anti-PPARα | Rockland Immunochemicals | Cat # 600-401-421; RRID:AB_2165756 |
| Rabbit polyclonal anti-LXR | Proteintech | Cat # 14351-1-AP; RRID:AB_10640525 |
| Rabbit polyclonal anti-RXRα | Cell Signaling Technology | Cat # 5388S; RRID:AB_10621998 |
| Rabbit monoclonal anti-HSP90 | Cell Signaling Technology | Cat # 4877S; RRID:AB_2233307 |
| Rabbit monoclonal anti- F4/80 antibody | Cell Signaling Technology | Cat # 70076S; RRID:AB_2799771 |
| Chemicals, peptides, and recombinant proteins | | |
| Oil Red O | Cayman Chemical | Cat # 14419 |
| D-(+)-glucose | Sigma | Cat #G7528 |
| Chow Diet (ProLab® RMH 3000) | LabDiet | Cat # 5P00 |
| High Fat Diet | Research Diets Inc. | Cat #D12451 |
| Low Fat Diet | Research Diets Inc. | Cat #D12450B |
| Critical commercial assays | | |
| Triglycerides Liquid Stable Reagent | Thermo Scientific | Cat # TR22421 |
| Total Cholesterol and Cholesteryl Ester Fluorometric Assay Kit | BioVision | Cat #K603-100 |
| Sirius Red Stain Kit | Abcam | Cat # ab150681 |
| Deposited data | | |
| RNA-seq data | This paper | GSE241875 |
| Mass Spectrometry data | This paper | PXD045279 |
| Experimental models: Organisms/strains | | |
| Mouse: *Huwe1*$^{fl/fl}$ | Kon et al.[15] | N/A |
| Mouse: B6.Cg-Speer6-ps1Tg(Alb-cre)21Mgn/J | Postic et al.[16] | RRID:IMSR_JAX:003574 |
| Software and algorithms | | |
| GraphPad Prism | GraphPad | https://www.graphpad.com/ |
| R: A Language and Environment for Statistical Computing | R Foundation for Statistical Computing | https://www.r-project.org/ |
| Molecular signatures database | Broad Institute | https://www.gsea-msigdb.org/gsea/msigdb |
| ImageJ | National Institutes of Health | https://imagej.nih.gov/ij/index.html |

## RESOURCE AVAILABILITY

### Lead contact

Further information and requests for resources and reagents should be directed to and will be fulfilled by the Lead Contact, Manabu Kurokawa (mkurokaw@kent.edu).

### Materials availability

All unique/stable reagents generated in this study are available from the lead contact with a completed Materials Transfer Agreement.

## Data and code availability

Raw and processed RNA-seq data was deposited in the Gene Expression Omnibus (GEO) database and are publicly available under the accession number GSE241875. Mass spectrometry data was deposited in the ProteomeXchange Consortium under project accession number PXD045279.

## EXPERIMENTAL MODEL AND STUDY PARTICIPANT DETAILS

### Mice

*Huwe1*$^{f/fl}$ mice were previously described.[15] Alb-Cre mice (B6.Cg-Speer6-ps1Tg(Alb-cre)21Mgn/J, Stock No: 003574[16]) were obtained from The Jackson Laboratory. All mice used in this study were on C57BL/6 background. In all experiments, nearly equal numbers of male littermates (WT and LKO) were included, and the results were pooled and analyzed. On average, 3–4 mice were housed per cage. Mice were maintained on 5P00 ProLab RMH 3000 (LabDiet) chow diet *ad libitum* until initiation of diet experiments. LFD (D12450B) and HFD (D12451) were purchased from Research Diets Inc. Body weights and diet weights were measured weekly. Body composition was measured using an EchoMRI-700 quantitative magnetic resonance body composition analyzer (Echo Medical Systems). All animal studies were performed by protocols approved by the Institutional Animal Care and Use Committee (IACUC) at Dartmouth College and Kent State University.

## METHOD DETAILS

### Glucose tolerance test

Glucose tolerance tests were performed as previously described.[43] Briefly, mice were fasted overnight for 16 h before intraperitoneal injection with 2 mg/kg D-glucose (Sigma). Blood glucose was measured 0, 15, 30, 60, 120 min post-injection using an Accu-Chek Aviva glucometer (Roche).

### Immunohistochemistry (IHC)

Livers were harvested and fixed in 10% neutral buffered formalin overnight before tissue dehydration and paraffin embedment. Tissues were sectioned in 10 μm slices and then dried at 60°C for 20 min. The tissues were then subsequently stained with Harris Hematoxylin (VWR) and Eosin (VWR) after deparaffinization with Xylene (VWR) and hydration. Slides were mounted using VectaMount AQ aqueous mounting media (Vector Laboratories). Slides were imaged by brightfield microscopy within 12 h of staining. Sirius red staining was performed using the Sirius Red Stain Kit (Abcam), according to the manufacturer's instruction. F4/80+ quantification shown in Figure 7L was conducted using ImageJ version 1.54d.

### ORO staining

Livers were harvested and fixed overnight in 10% neutral buffered formalin. Tissues were rinsed in PBS followed by 48 h incubation in 20% sucrose at room temperature. Tissues were then frozen in optimal cutting temperature (OCT) compound (Tissue-Tek) followed by sectioning into 8 μm slices. Tissue sections were then dried at room temperature, followed by staining in ORO (Cayman Chemical) working solution for 5 min. Slides were then rinsed in deionized water followed by a 10-min incubation with Mayer's Hematoxylin (Sigma-Aldrich). Slides were washed in deionized water and mounted using VectaMount AQ aqueous mounting media (Vector Laboratories). Slides were imaged by brightfield microscopy within 6 h of staining.

### Triglyceride and cholesterol quantification

Livers were homogenized in 500 μL PBS followed by the addition of 700 μL chloroform:isopropanol:NP-40 (7:11:0.1 proportion). Mixtures were vortexed and incubated in a sonicating water bath for 1 h. Eppendorf tubes were vortexed, then spun at 13,000 rpm for 10 min. The lower organic phase containing liver lipid extracts was isolated and dried. Hepatic triglyceride levels were measured using Infinity Triglycerides Liquid Stable Reagent (Thermo Scientific) and total cholesterol levels were measured using Total Cholesterol and Cholesteryl Ester Fluorometric Assay Kit (BioVision) according to manufacturer's instructions.

### RNA-seq

RNA was isolated using the SV Total RNA Isolation System (Promega, cat no. Z3105) in accordance with the manufacturer's recommendations. Library prep was performed by BGI Genomics (San Jose, CA). RNA-seq was performed using the BGISEQ-500 platform. Clean reads were mapped to a reference genome using Bowtie2, and gene expression was calculated using RSEM. DEseq2 was used to identify differentially expressed genes with significance set at *$p < 0.05$ after Benjamini-Hochberg correction for multiple comparisons. Hallmark gene set enrichment analyses were performed using the molecular signatures database (MSigDB) v7.2.

### Real-time quantitative PCR (RT-qPCR)

RT-qPCR was performed as previously described.[44] RNA was isolated using an SV Total RNA Isolation System (Promega) according to the manufacturer's instructions. cDNA was synthesized using a qScriptTM cDNA synthesis kit (Quanta). RT-qPCR was performed using iTaq Universal SYBR Green Supermix (Bio-Rad) on a CFX96TM Real-Time Detection System. The data was analyzed using the Delta-Delta Ct Method,

and individual gene expression was normalized to the expression of *Rplp0*. The RT-qPCR primers were purchased from Integrated DNA Technologies. The corresponding sequences are listed in Table S7 [List of primers used for RT-qPCR].

### Western blot

Cells were lysed in RIPA buffer supplemented with protease and phosphatase inhibitors (Roche). Lysates were cleared by centrifugation at 20,000g for 20 min at 4°C and 40 μg protein was loaded per lane on 8% polyacrylamide gels. Proteins were transferred onto PVDF membranes (Millipore) and were blocked in 3% BSA for 30 min at room temperature. Membranes were incubated with primary antibodies overnight at 4°C with gentle agitation. Membranes were developed using Pierce ECL (Thermo Scientific) and X-ray film. Band densitometry was conducted using ImageJ version 1.54d.

### Sample preparation for proteomics analysis

Hepatic proteins (100 μg) from frozen liver tissues were fractionated with sodium dodecyl sulfate polyacrylamide gel electrophoresis (SDS-PAGE) for 10 min at 150 V. One wide gel band corresponding to a mixture of hepatic proteins was cut and processed for proteomic analyses. Extracted gel bands were reduced with dithiothreitol (DTT), alkylated with iodoacetamide and digested with trypsin (Promega, Madison, WI) at 37°C overnight. The tryptic peptides were extracted from polyacrylamide gel bands in a sonication bath with 100 μL of 40% acetonitrile with 0.1% trifluoroacetic acid (TFA) and 100 μL of 70% acetonitrile with 0.1% TFA, consecutively. In-gel digested tryptic peptides were analyzed by nanospray LC-MS/MS after reconstitution in 0.1% formic acid.

### LC-MS/MS analysis

A solution of tryptic peptides was analyzed by Ultimate 3000 UHPLC (Thermo Scientific, CA) coupled online to Q Exactive Plus Hybrid Quadrupole-Orbitrap Mass Spectrometer (Thermo Scientific, CA). After desalting samples on an Acclaim PepMap100 precolumn (300 μm × 5 mm, C18, 5 μm, 100 Å, Thermo Fisher Scientific), peptides were separated on an Acclaim PepMap RSLC reverse phase nano-column (75 μm × 15 cm, C18, 2 μm, 100 Å, Thermo Fisher Scientific) at 300 nL/min with a mobile phase A (0.1% formic acid in water) and B (20% water in acetonitrile with 0.1% formic acid). A stepwise gradient was employed with an initial 2% of mobile phase B. After 4 min of de-salting, mobile phase B was linearly increased to 35% in 90 min. Mobile phase B was then ramped to 90% in 5 min and then held at 90% B for 10 min. Subsequently, mobile phase B was decreased to 2% for 2 min and equilibrated for 13 min with 2% of phase B.

Mass spectrometry analysis was performed in data-dependent acquisition mode with a full profile MS scans at 70000 resolution (200 m/z) between 380 and 1300 m/z. MS/MS spectra were collected in data-dependent acquisition mode for the 14 most abundant precursor ions with an isolation window of 1.4 and offset of 0.3 m/z and 17,500 resolution (at 200 m/z). Higher-energy collisional dissociation (HCD) was performed at a normalized collision energy of 25%. The precursor ion masses were dynamically excluded from MS/MS analyses for a duration of 20 s. MS and MS/MS spectra were acquired for 100 ms with the automatic gain control (AGC) target set at 1.0 x 106 and 2.0 x 104 ions for MS and MS/MS scans, respectively.

For protein identification, all the spectra obtained from the mass spectrometer were transformed into mzML file format using ProteoWizard MSconvert Version 3.0.18116 (http://proteowizard.sourceforge.net/tools), and the MZML files were searched using Mascot software (Matrix Science, London, UK) version 2.3 against the mouse subset of the UniProt protein database released on June 29th, 2016 (containing 149,730 entries) with cysteine carbamidomethylation as fixed and methionine oxidation as variable modifications and trypsin digestion with a maximum of two missed cleavages per peptide.

To assess HUWE1-induced relative changes in hepatic proteins levels, tryptic peptides from both groups were quantified using MaxQuant software (MaxQuant V1.5.2.8)1. Raw files were searched using MaxQuant-integrated Andromeda search engine (version 1.5.2.8) using the parameters for the Orbitrap instrument as default settings. MaxLFQ algorithm of MaxQuant measures the area under the curve of high intensity paired peptides' signals from multiple samples in each group. The MaxQuant results were manually validated using Xcalibur software (version 3.1, Thermo). To account for variations during sample preparation, peptides isolated from equal total protein amounts (30 μg) were quantified. Data were Log2 transformed and were normalized relative to the mean of control group. Comparison between groups was then estimated as fold change. Thus, the results of these measurements represent relative levels of proteins in whole tissue lysate and reflect the HUWE1-induced change in expression rather than the absolute concentrations of analyzed proteins.

The results were summarized using means and standard deviations and were compared between groups using two-sample t-tests. Mean differences between groups with 95%-confidence intervals were presented.

### Statistical analysis

Two-tailed Student's *t* test was used to determine statistical significance between groups using GraphPad Prism v8.3.1. Growth curve analysis was conducted using the "statmod" R package with significance set at *$p < 0.05$ after Benjamini-Hochberg correction for multiple comparison. Analyses were run in R version 3.4.2. Further statistical details of experiments can be found in the figure legends.